Broadly reactive anti-VHH antibodies for characterizing, blocking, or activating nanobody-based CAR-T cells

McComb, Scott; Dupont, Bianca; Shepherd, Alex; Bennychen, Bigitha; Marcil, Anne; Tamblyn, Laura; Raphael, Shalini; Sheff, Joey; Hussack, Greg; Moraitis, Anna N; Wu, Cunle; Aubry, Annie; Gadoury, Christine; Lippens, Julie; Pagé, Martine; Fortin, Annie; Joubert, Simon; Lamoureux, Linda; Parat, Marie; Plante, Pierre; Malenfant, Félix; Acchione, Mauro; Pohankova, Petra; Schrag, Joe; Acel, Andrea; Coutu, Mathieu; Smith, Emma; El Bakkouri, Majida; Hill, Jennifer J; Tremblay, Tammy-Lynn; Manceur, Aziza P; Faulkes, Sharlene; Webb, John; Zafer, Ahmed; Zhu, Qin; Nguyen, Tina; Pon, Robert A; Weeratna, Risini D; Arbabi-Ghahroudi, Mehdi

Publisher's version / Version de l'éditeur:

https://doi.org/10.1093/abt/tbaf011

Antibody Therapeutics, 8, 3, pp. 242-258, 2025-06-27

OXFORD

Antibody Therapeutics, 2025, 8(3), 242–258
https://doi.org/10.1093/abt/tbaf011
Advance access publication date 27 June 2025
Research Article

Broadly reactive anti-VHH antibodies for characterizing, blocking, or activating nanobody-based CAR-T cells

Scott McComb[1,2,3,4,*], Bianca Dupont[2], Alex Shepherd[2], Bigitha Bennychen[2], Anne Marcil[1], Laura Tamblyn[1], Shalini Raphael[1], Joey Sheff[1,2], Greg Hussack[1], Anna N. Moraitis[1,5], Cunle Wu[1,5], Annie Aubry[1,5], Christine Gadoury[1], Julie Lippens[1,5], Martine Pagé[1,5], Annie Fortin[1,5], Simon Joubert[1], Linda Lamoureux[1], Marie Parat[1], Pierre Plante[1], Félix Malenfant[1], Mauro Acchione[1], Petra Pohankova[1], Joe Schrag[1], Andrea Acel[1], Mathieu Coutu[1], Emma Smith[1], Majida El Bakkouri[1], Jennifer J. Hill[1,4], Tammy-Lynn Tremblay[1], Aziza P. Manceur[1], Sharlene Faulkes[6], John Webb[7], Ahmed Zafer[1], Qin Zhu[1], Tina Nguyen[1], Robert A. Pon[1], Risini D. Weeratna[1], Mehdi Arbabi-Ghahroudi[1,2]

[1]Human Health Therapeutics Research Centre, National Research Council Canada, Montreal, QC, H4P 2R2, and Ottawa, ON, K1A 0R6, Canada
[2]Department of Biochemistry, Microbiology and Immunology, Faculty of Medicine, University of Ottawa, Ottawa, ON, K1H 8M5, Canada
[3]Centre for Infection, Immunity, and Inflammation, University of Ottawa, Ottawa, ON, Canada
[4]Ottawa Institute for Systems Biology, Ottawa, ON, K1H 8M5, Canada
[5]Medical Devices Research Centre, National Research Council Canada, Boucherville, QC, J4B 6G4, Canada
[6]Department of Pathology and Laboratory Medicine, Faculty of Medicine, University of Ottawa, Ottawa, ON, K1H 8M5, Canada
[7]Deeley Research Centre, British Columbia Cancer Research Institute, Victoria, BC, V8R 6V5, Canada
*Corresponding author. Human Health Therapeutics Research Centre, National Research Council Canada, Ottawa, ON, K1A 0R6, Canada.
E-mail: scott.mccomb@nrc-cnrc.gc.ca

Abstract

Background: Production of chimeric antigen receptor T cell (CAR-T) therapies depends on antibody reagents to label, isolate, and expand T cell products. We sought to create antibody tools specific for the variable domain of heavy-chain only antibodies (VHHs), also known as nanobodies, used in some CARs.
Methods: We immunized a mouse with VHH and selected two murine monoclonal antibodies (mAbs) that bind to distinct epitopes in conserved framework regions of llama-derived VHHs, and not to human VH domains. Anti-VHH mAbs were characterized by enzyme-linked immunosorbent assay, surface plasmon resonance, and hydrogen-deuterium exchange mass spectrometry; were then tested for cell/tissue labeling and for modulating cellular activity in VHH-CAR-T cells.
Results: We produced a high-quality dual-clonal anti-VHH antibody product and confirmed reactivity to over 98% of VHH proteins regardless of their antigenic specificity, with no reactivity to human or mouse IgG and reduced reactivity to conventional llama or alpaca IgG. Anti-VHH binding did not disrupt VHH/antigen interaction, and thus was appropriate for secondary labeling to assess cellular or tissue reactivity of VHH molecules. Despite not interfering with antigen binding, anti-VHH antibodies (Abs) potently blocked VHH-CAR-T activation and cytolytic killing of target cells. When immobilized, anti-VHH Abs induced strong activation and expansion of VHH CAR-T cells; with 730-fold mean expansion, >94% CAR purity, and retained CD8/CD4 heterogeneity. Functionally, anti-VHH antibody-expanded CAR-T cells maintained strong antigen-specific activity without functional exhaustion.
Conclusions: Overall, these data identify useful anti-VHH mAbs that can be applied to better understand and manipulate VHH-based CAR-T cells or other VHH-based immunotherapies.

Statement of Significance
Antibody tools are foundational to discovery and development of engineered cell therapies; here we report broadly reactive anti-variable domain of heavy-chain only antibodies that can be used to quantify, isolate, inhibit, or activate T cells expressing llama nanobody chimeric antigen receptors.

Keywords: Nanobodies; VHH; Chimeric Antigen Receptors; CAR-T; CAR labeling

Introduction

The development of CD3-targeting antibodies (Abs) was a pivotal step toward creating a standardized method for expanding T-cells, eventually leading to the development of modern T-cell therapies such as chimeric antigen receptor (CAR) T-cell therapy. As with other receptor-targeting Abs, soluble CD3-specific Abs can block antigen-specific stimulation of T-cells through the T-cell receptor (TCR), whereas when these same anti-CD3 Abs are multimerized,

Received: November 21, 2024. **Revised:** April 1, 2025. **Accepted:** April 22, 2025

they will act as potent activators of T-cell proliferation [1, 2]. Cross-linking of anti-CD3-Abs, either through Fc-conjugation [3], surface absorption [4], multimerization [5, 6], artificial antigen-presenting cells [7], or bead conjugation [8], are all proven strategies to exploit the T-cell activating properties of anti-CD3-Abs. In addition to altering T-cell receptor signaling, anti-CD3 Abs are among a plethora of Abs that are directly conjugated to chemical fluorophores for identification of T cells via flow cytometry and/or cell isolation via magnetic or flow-based cell sorting.

Given the indispensability of CD3-targeted Abs to the scientific and clinical development of T cell therapies, we reasoned that establishing a standardized Ab-based reagent targeting the antibody framework domains within the antigen-binding domain of CAR-T receptors could have similar multifaceted utility for the development of CAR-T therapies. Specifically, our focus has been on the development of CAR therapies utilizing variable domains of llama heavy-chain only antibodies (VHHs), which are also known as nanobodies. VHHs have several advantages over single-chain variable fragment domains (scFvs), which are more widely used in CAR therapies, including a simpler single-gene structure, smaller size, and higher genetic homology to human variable domains than mouse or rabbit Abs [9]. We have recently reported on novel VHH-based CAR molecular discovery and optimization for VHH-CARs targeting the epidermal growth factor receptor (EGFR) and CD22 [10, 11]. The most clinically advanced application of VHH binding domains in a CAR is in ciltacabtagene autoleucel, a B-cell maturation antigen (BCMA)-targeted CAR-T product now approved as a marketed treatment of multiple myeloma in a growing number of countries [12].

Here, we sought to identify murine monoclonal antibodies (mAbs) that can selectively bind to llama-derived VHHs of various VHH-CAR proteins, without cross-reacting with human or mouse-derived Abs, and explore their potential applications. We produced a high-quality and consistent mAb product that can be used as a secondary anti-VHH staining reagent to characterize VHH binding to antigen-expressing target cells, or to quantify surface expression of VHH-CARs. These mAbs show broad reactivity to almost all VHHs tested, regardless of their antigenic specificity. In addition to staining applications, we also find that anti-VHH mAbs can recapitulate other functions of CD3-specific Abs, such as blockade of antigen-specific response or activating specific expansion of VHH CAR-T cells.

Results

Identification of broadly cross-reactive anti-VHH mAbs

In order to generate mAbs specific for VHH domains, a previously reported blood–brain barrier transmigrating VHH (clone FC5) [13] was produced and purified from bacterial culture via affinity column purification. Four A/J mice were then immunized with VHH emulsified in TiterMax adjuvant and boosted with VHH before harvesting spleens. Hybridoma cultures were then generated via electrofusion and clone screening for VHH binding as previously reported [14]. A total of 233 hybridoma supernatants were screened, revealing 37 supernatants with reactivity to FC5. To avoid potential problematic reactivity with human Abs in downstream application, 31 of 37 hybridoma supernatants were specifically selected for negative reactivity via enzyme-linked immunosorbent assay (ELISA) against polyclonal human IgG-containing serum (Fig. 1A, Supplemental Table 1). Of the 31 remaining hybridoma supernatants, only 10 showed broad reactivity to 3 llama VHHs tested via ELISA. Finally, seven supernatants were further selected based on hybridoma growth and antibody productivity characteristics.

As our primary intent for generating anti-VHH mAbs was for surface labeling of VHH-CAR expressing cells, we first confirmed reactivity of all seven candidate supernatants to Jurkat cells stably expressing a VHH-CAR via flow cytometry (Fig. 1B). Next, we performed the same analysis using primary human CAR-T cells from two healthy donors, generated via lentiviral transduction of varying CARs as reported previously [15]. Results revealed varying reactivity to VHH-CAR expressing cells, with two particular mAb supernatants (clones 2A3 and 3H12) showing strong and consistent reactivity across all 5 VHH-CARs tested (Fig. 1C). Neither anti-VHH mAb supernatant showed reactivity against control murine and human scFv-CARs, FMC63 and m971, or against unmodified mock transduced T cells. Overall, these results identified two promising candidate anti-VHH mAbs with broad reactivity to VHH domains.

Production and testing of recombinant anti-VHH mAbs

Having selected two candidate anti-VHH mAbs, the heavy and light chain variable genes were sequenced from 2A3 and 3H12 mAb IgG1 hybridoma clones. The variable domains from these clones were then recombined to mouse IgG2a-Fc backbones. It has been our experience that murine IgG2a Abs result in higher antibody production and have better stability. Binding to purified VHH shows that recombinant IgG2a anti-VHH (rec2A3 and rec3H12) mAbs maintain similar reactivity to VHH as the original IgG1 mAbs (Supplemental Fig. 1A). We also confirmed that the recombinant IgG2a anti-VHH mAbs maintain low reactivity to human IgG (Supplemental Fig. 1B). As product quality and consistency is vital for use in downstream pre-clinical and clinical processes of CAR-T, we also confirmed inter-batch consistency, freeze–thaw stability, and stability over at least 12 months in −80°C storage for this product (Supplemental Fig. 1B–F). Given these strong product quality and consistency observations, we used the recombinant IgG2a forms of anti-VHH mAbs for further characterization and application studies discussed throughout the remainder of this manuscript.

Recombinant anti-VHH mAbs were then directly labeled with AlexaFluor-647 and tested to confirm reactivity to VHH-CAR expressing cells in various applications. Importantly, early testing revealed that certain VHH-CAR molecules were not labeled efficiently with 3H12 (EGFR-CAR, Supplemental Fig. 2A) or 2A3 (CD22-CAR, Supplemental Fig. 2B) respectively. We thus hypothesized that a 1:1 mix of both anti-VHH mAbs would provide a more consistent staining reagent that could be applied across varying VHH-CAR molecules. Indeed, titration of a mixed anti-VHH product revealed a uniform staining profile in the two VHH-CARs tested here (Supplemental Fig. 2A, B).

To confirm consistent reactivity of this anti-VHH mAb mixture against more VHH-CAR molecules, six additional VHH-CAR-expressing Jurkat T cell lines with specificity for four distinct surface targets (BCMA, mesothelin, CD22, and CD20) were stained and analyzed by flow cytometry. Across the six additional VHH-CARs, staining with the anti-VHH mAb mix correlated directly with the NeonGreen fluorescent marker co-expressed with VHH-CAR genes (Supplemental Fig. 2C). Similarly, we were also able to use the anti-VHH mAb mix to confirm CAR expression in NK92-IL15 cells transduced with a VHH-CAR lentivirus, wherein stable GFP expression precluded the use of NeonGreen to quantitate CAR expression (Supplemental Fig. 2D). A similar application of anti-VHH mAbs would be to perform a rapid quantification of lentiviral

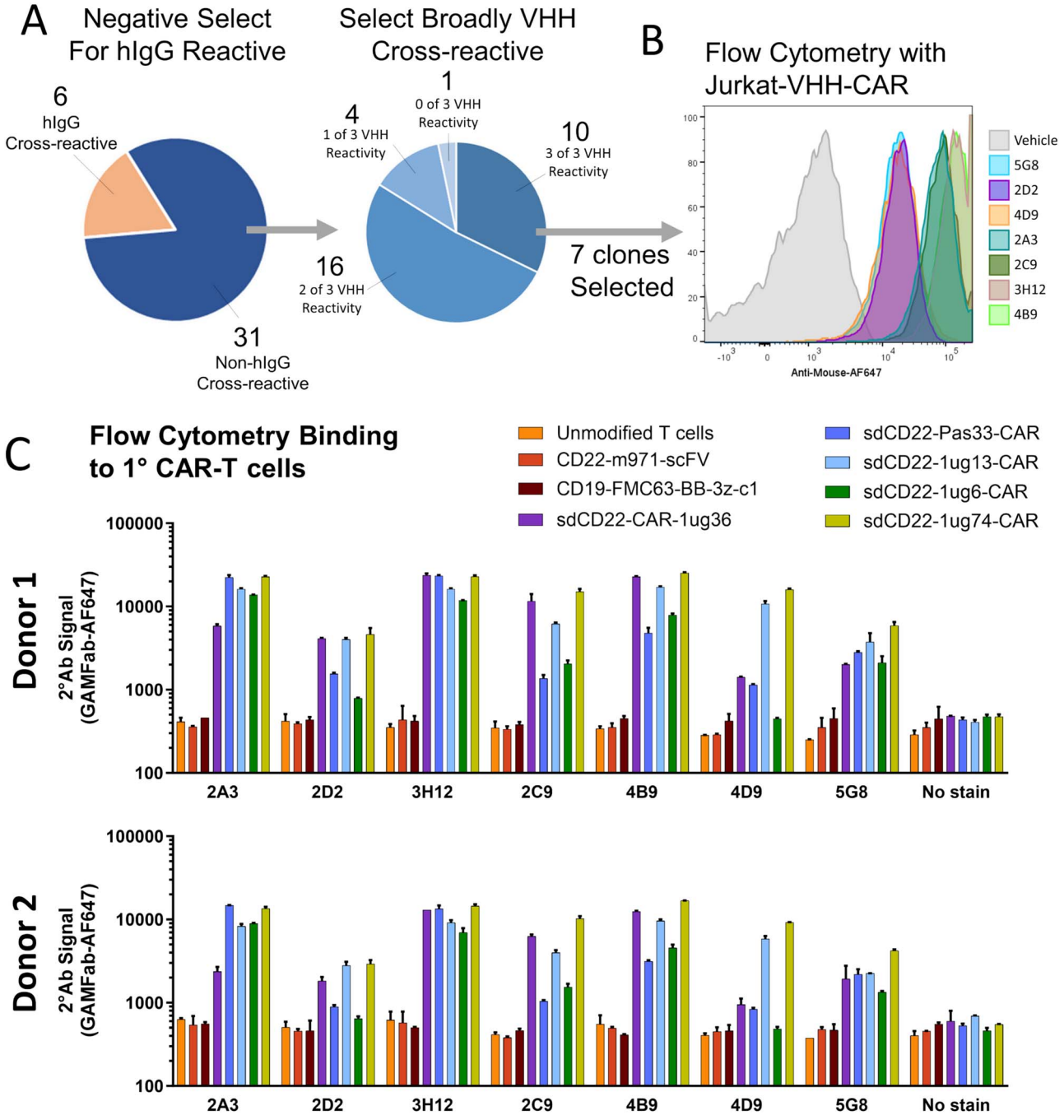

Figure 1. Selection of two broadly cross-reactive mouse anti-VHH mAbs by mouse immunization with a purified VHH. (A) Clonal hybridoma culture supernatants were screened via ELISA for reactivity to human total IgG protein, selecting only those with negative reactivity to human IgG for further testing. Non-human reactive supernatants were then screened via ELISA for cross-reactive binding to three different VHHs, with a total of 10 clones showing reactivity to 3 of 3 VHHs. (B) Flow cytometry was then conducted with Jurkat cells bearing stable expression of surface-linked VHH-chimeric antigen receptor (Jurkat-VHH-CAR) to confirm the reactivity of seven selected anti-VHH hybridoma supernatants. (C) Anti-VHH hybridoma supernatants were similarly screened for reactivity against primary CAR-T cells from two different healthy donor blood samples expressing five different VHH-CARs, two control scFv-CARs, or untransduced T cells. Bar graphs show the median fluorescence intensity of anti-VHH staining on gated EGFP+ CAR-expressing cells from one experiment performed in duplicate +/− SEM. Supernatants with the broadest cross-reactivity (2A3 and 3H12) were selected for downstream testing.

particle production for a VHH-CAR lentivirus without the need to express a fluorescent marker gene (Supplemental Fig. 2E). Overall, these results indicate that a mixed product of anti-VHH mAbs can be used to quantify surface expression of VHH-CAR molecules with divergent variable domain sequences and antigen specificity.

Anti-VHH mAbs show differential reactivity with purified VHH proteins

Next, we wanted to confirm the breadth of reactivity with a large panel of VHHs. We performed an ELISA, wherein a wide array of VHHs, generated over 8 independent VHH discovery projects targeting 11 unique antigens, were tested for binding with our

anti-VHH mAbs. VHHs were absorbed onto ELISA plates and probed with 3H12, 2A3, or a 1:1 mix of both mAbs, detecting anti-VHH mAb reactivity with an anti-mouse secondary Ab. We found that 75 of 76 unique VHHs are recognized by the 1:1 mix of anti-VHH mAbs; 74 of 76 are recognized by 3H12 mAb; and 73 of 76 are recognized by 2A3 mAb (Fig. 2A). Both mAbs reacted with a recently reported llama VH domain [16], which was monomeric but distinct in sequence from a typical VHH (Fig. 2B). Importantly, we did observe examples wherein 3H12 or 2A3 each showed greater reactivity, such as VHH-59 or VHH-60, respectively, with the mix being the most broadly reactive (Fig. 2A, C). Surface plasmon resonance (SPR) assays, using VHHs as analytes flowed over anti-mouse Fc captured 3H12 and 2A3 mAbs, revealed a similar pattern of reactivity to the ELISAs for a representative set of VHHs (Fig. 2D), with monovalent binding affinities ranging from K_D = 3.9 – 9.5 nM and K_D = 2.4 – 192 nM for 3H12 and 2A3, respectively.

Following these results, we performed a sequence alignment of the 76 VHHs used in ELISA to identify potential sequence determinants associated with positive or negative anti-VHH mAb reactivity. As expected, the framework regions (FRs) showed a broad consensus between the VHHs (Supplemental Fig. 3). For 3H12, we observed weak or negative reactivity with 5 of 5 VHHs with a serine substitution in position 11 in FR1 of the VHH (Fig. 2E). Introduction of an S11L mutation into VHH-53 was able to restore 3H12 binding (Fig. 3F), pinpointing residue 11 as a key interaction for 3H12. For 2A3, we were unable to identify any consensus FR sequences that were associated with positive or negative binding; however, a motif in FR2 was identified as a potential region important for 2A3 binding (Fig. 2E). Overall, these data indicate that the anti-VHH mAbs generated here show broad reactivity with llama VHHs, likely through recognition of distinct epitopes within the FRs of llama VHHs.

Anti-VHH mAbs show species-dependent reactivity

In order to confirm the reactivity of anti-VHH mAbs reported here, we performed ELISA against whole serum from llama, alpaca, human, and mouse. As expected, we observed strong reactivity to sera from llama and alpaca, species where VHH are found. We observed no reactivity to human or mouse sera (Fig. 3A). To confirm whether reactivity is selective for camelid VHH over conventional VH/VL Abs in camelid sera, we performed serum fractionation. SDS-PAGE analysis confirmed that conventional VH/VL was only found in the G2 serum fraction for all species, whereas other fractions from llama and alpaca (G1, A1, and A2) contained VHH proteins (Fig. 3B). ELISA revealed the strongest binding to VHH-containing fractions from llama and alpaca, with ~10× lower reactivity to camelid G2 fractions, wherein conventional IgG is found (VH/VL; Fig. 3C). As with whole serum, reactivity was confirmed to be low for both mouse and human serum fractions. In summary, this data demonstrates VHH-selectivity, especially in the context of mouse or human IgG, although these anti-VHH mAbs should not be used as a tool to specifically confirm VHH in the context of whole camelid sera due to their partial reactivity with conventional camelid VH/VL proteins.

Hydrogen deuterium exchange mapping of anti-VHH mAbs mapping reveals distinct but competitive epitopes

To further investigate how the anti-VHH mAbs interact with VHHs, we generated a yeast surface display (YSD) library with progressively truncated VHHs, probing with anti-VHH mAbs via whole-cell ELISA. Consistent with our observations in the VHH ELISA above, both 2A3 and 3H12 showed strong binding in a whole-cell ELISA using yeast displaying a cell-wall-linked VHH protein. Binding with 3H12 was completely lost with an N-terminal 15 amino acid truncation of the VHH FR1 (Fig. 4A, B), but 2A3 maintained partial reactivity. Both mAbs showed negative reactivity to a 21-amino acid or greater truncation. C-terminal truncations also showed negative reactivity, but we hypothesize that many of these truncations likely lead to severe misfolding and/or instability of the VHH in YSD. Nonetheless, these data provide supporting evidence that 2A3 and 3H12 show differential binding and likely target distinct epitopes.

To more finely map the anti-VHH mAb epitopes, we employed hydrogen deuterium exchange mass spectrometry (HDX-MS). Deuteration was measured for 41 peptides covering >80% of the CD22-specific VHH (clone 1ug36, 10) test material (Supplemental Fig. 4). Results show that saturation of the VHH with 3H12 but not 2A3 resulted in a slower exchange of hydrogen atoms mostly within the N-terminal amino acids of FR1 of the VHH (residues S6–S17), corroborating our YSD findings (Fig. 4B, Supplemental Table 2). Additionally, 3H12 slowed HDX for residues within FR2 (Q39-E46) and FR3 (V63-F67), suggesting a discontinuous epitope spanning multiple framework loops that are distal from the hypervariable complementarity-determining regions (CDRs). Saturation of the VHH protein with 2A3 mAb only resulted in slower HDX within the FR2 region (Fig. 4B). Both VHH proteins exhibited faster exchange in residues D89-Y94 (red, Fig. 4B), which likely results from allosteric conformational changes induced by stabilization of the framework loops.

Competitive SPR binding experiments involving sequential anti-VHH mAb injections over an amine-coupled VHH surface revealed 2A3 and 3H12 partially competed with one another, with binding of the first mAb preventing full unobstructed binding of the second mAb (Fig. 4C). Given the much larger size of the mAbs compared to a VHH (~10× larger), the inability of the anti-VHH mAbs to simultaneously bind with a VHH is unsurprising. Collectively, our sequence analyses, ELISA, YSD, HDX-MS, and SPR results indicate that the anti-VHH mAbs recognize two distinct but adjacent epitopes within the conserved FR domains of VHHs, which are distal from the CDR.

Anti-VHH mAbs for assessment of VHH cellular reactivity

Based on our epitope mapping experiments, we expected that anti-VHH mAb binding should not disrupt CDR-mediated VHH-antigen interaction; thus, we wanted to confirm whether these mAbs could be applied to investigate cellular reactivity of soluble VHH proteins. Antigen-expressing or deficient cells were stained with varying concentrations of VHHs, washed, and then probed with a fluorophore-conjugated anti-VHH mAb mix. Flow cytometry assessment showed specific reaction of anti-CD22 VHHs with CD22 expressing cells but not CD22-knockout cells (Fig. 5A). Similarly, BCMA-specific VHHs showed reactivity to a human multiple myeloma cell line, but not against BCMA-negative human Jurkat T cells (Fig. 5B). To see whether a similar technique could be applied to examine the tissue distribution of VHH binding, we also tested an immunohistochemistry (IHC) staining method using an anti-mouse-HRP polymer tertiary antibody detection reagent (Fig. 5C). Using this method, human tonsillar samples stained with CD22-specific VHHs revealed characteristic follicular staining pattern consistent with human B cells. These results demonstrate that anti-VHH mAbs are effective for characterization of cell and tissue binding of novel VHHs.

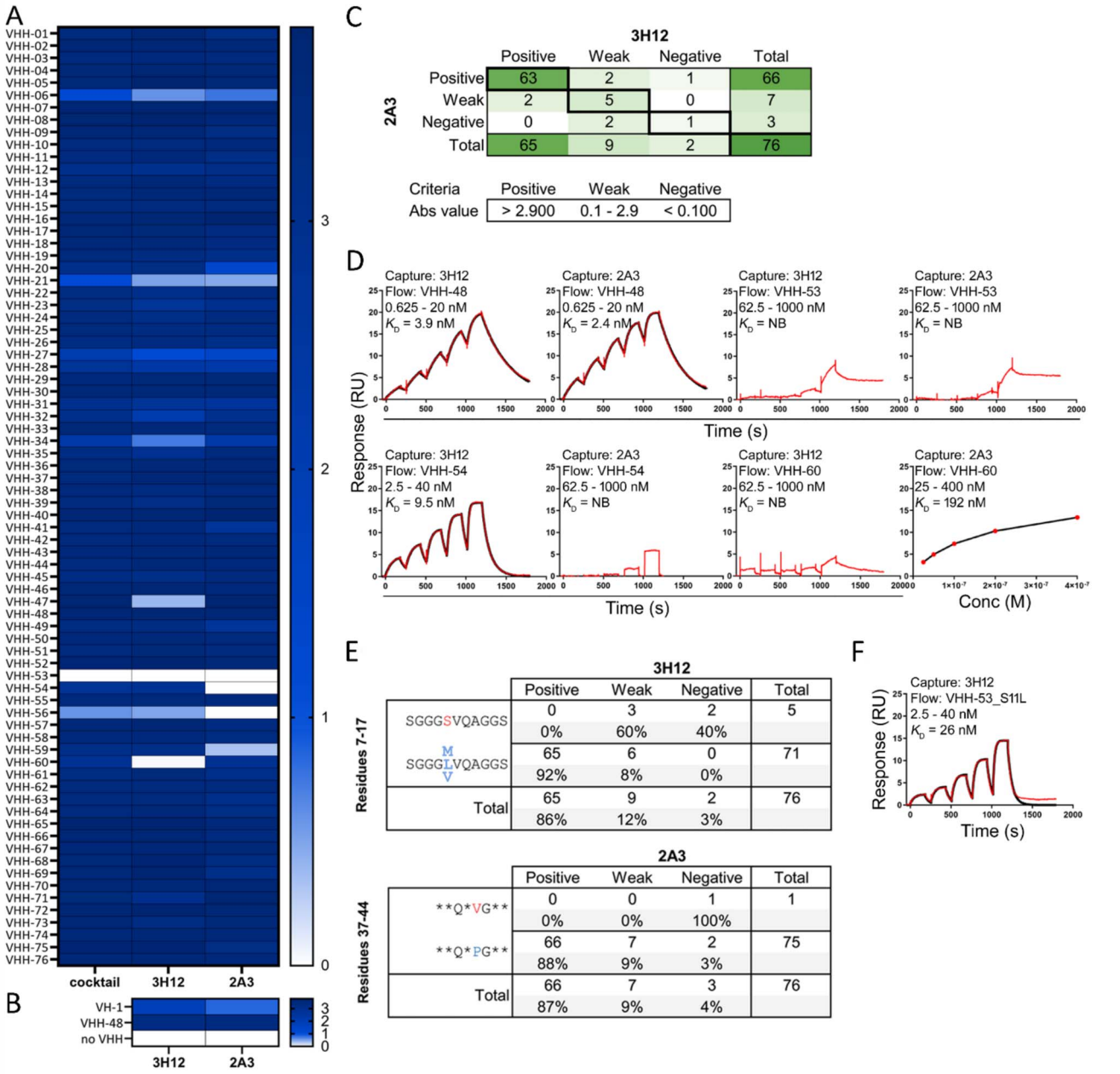

Figure 2. ELISA and SPR-based reactivity of 3H12 and 2A3 mAbs. (A) ELISA demonstrating 3H12 and 2A3 reactivity toward 76 passively absorbed llama-derived VHHs ("Cocktail" refers to an equimolar mix of 3H12 and 2A3); binding of mAbs to VHHs was detected with donkey-anti-mouse IgG-HRP as shown with absorbance readings at 450 nm. (B) Similarly, reactivity of 3H12 and 2A3 to a llama-VH domain, or a control VHH domain, was tested via ELISA, (C) summary of VHH detection by 3H12 and 2A3. (D) SPR sensorgrams showing monovalent binding affinities of select VHHs for mAbs. 3H12 and 2A3 mAbs were captured, and VHHs flowed at the concentration ranges indicated. NB: no binding. (E) VHH consensus sequences in FR1 (3H12) and FR2 (2A3) that may be predictors of mAb reactivity. (F) SPR sensorgram showing a single S11L mutation in FR1 of VHH-53 imparts 3H12 binding.

Soluble anti-VHH mAb binding can block VHH-CAR reactivity

Having demonstrated that anti-VHH mAbs can bind to both soluble and CAR-linked VHH moieties, we next wanted to assess how soluble anti-VHH mAbs would affect VHH-CAR response to antigen-expressing target cells. Jurkat cells with stable expression of a previously reported EGFR-specific VHH-CAR [11] were co-incubated with EGFR-positive human H292 lung cancer cells (Fig. 6A). EGFR-CAR Jurkat cells expressed high levels of the activation marker CD69 in the presence of H292 cells, whereas the addition of increasing doses of anti-VHH mAbs blocked CD69-upregulation with an IC_{50} of ~0.1 nM for the anti-VHH mAb mix (Fig. 6B). Similarly, in primary CAR-T cells transduced with EGFR-VHH CAR lentivirus, soluble anti-VHH mAb treatment resulted in a dose-dependent blockade of CAR-T activation, as assessed by the CD69 and CD25 activation markers (Fig. 6C). Furthermore, we observed potent inhibition of EGFR-VHH CAR-T cytolytic killing of EGFR-positive SKOV3 ovarian cancer cells with soluble anti-VHH mAb treatment (Fig. 6D, E). These results show that anti-VHH mAbs can be employed to block antigen-specific VHH-CAR function.

Immobilized anti-VHH mAb can activate and expand VHH-CAR cells

We next wanted to assess whether immobilization through surface absorption of anti-VHH mAbs could be used to specifically

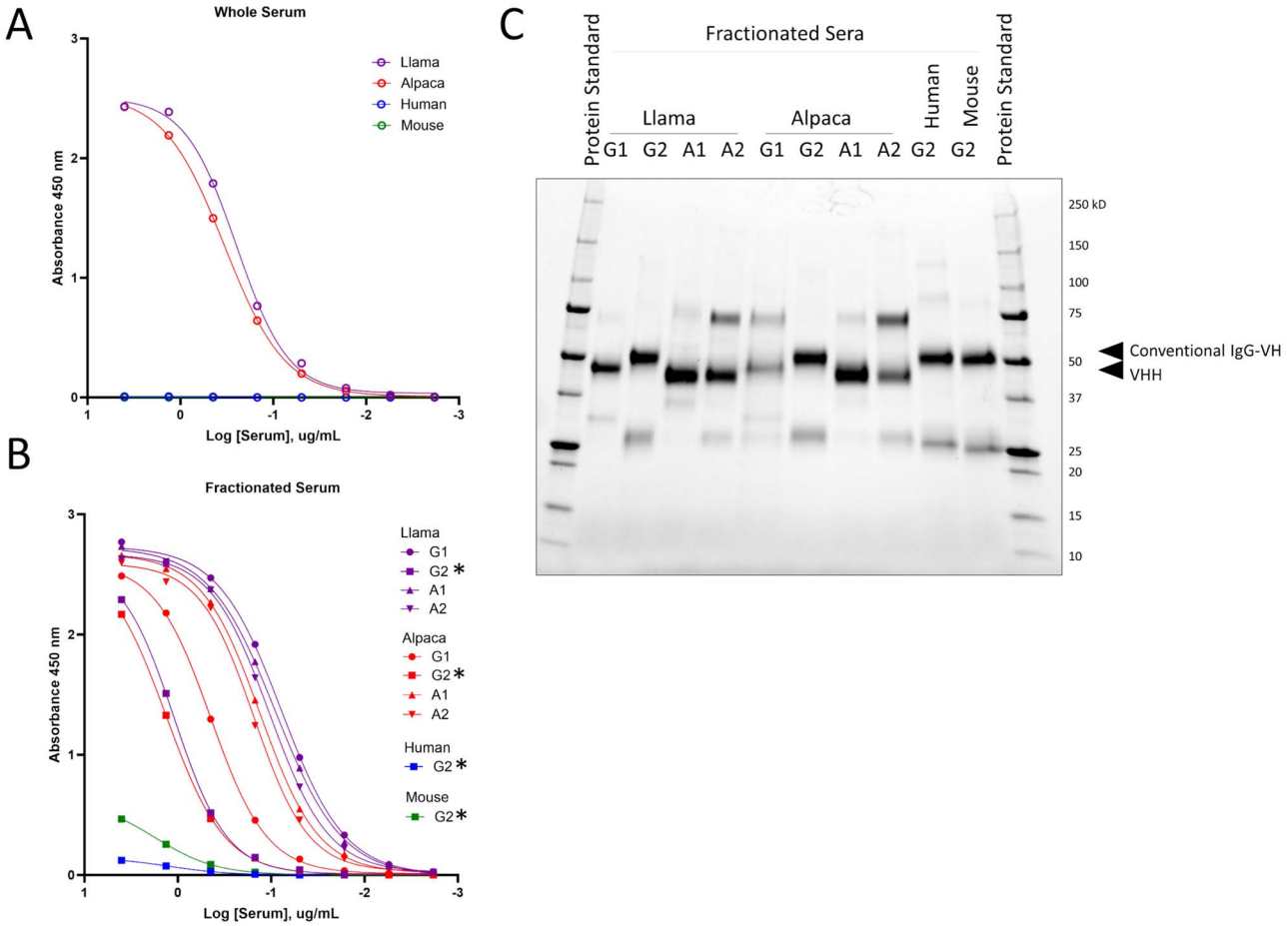

Figure 3. Anti-VHH mAbs are most reactive to VHH fraction of llama or alpaca serum. (A) Whole serum from human, mouse, and the camelid species llama, llama glama, and alpaca, *Vicugna pacos*, were assayed by protein ELISA to determine the species reactivity with a cocktail of antibody clones 2A3 and 3H12. (B) Similarly, 2A3 and 3H12 cocktail was examined via ELISA for reactivity to fractionated serum antibodies from llama, alpaca, human, and mouse. (C) Serum fractions were analyzed by SDS-PAGE to demonstrate that conventional IgG1 antibodies were isolated in the G2 fraction of serum from all species, while camelid heavy chain antibodies were isolated in the G1, A1, and A2 fractions of llama and alpaca serum. ∗*Asterisks denote fractions where conventional VH/VL antibodies are expected.*

expand CAR-T cells, similarly to what is commonly performed with CD3-specific mAbs. Upon exposure to various doses of plate-bound anti-VHH mAbs, we observed a dose-dependent upregulation of the T-cell activation marker CD69 in EGFR-VHH CAR-Jurkat cells but not in unmodified wild-type (WT) Jurkat cells (Fig. 7A, B). Interestingly, anti-VHH mAb activation in this case resulted in a lower magnitude of activation than with plate-bound anti-CD3 mAb. To investigate the consistency of this activation across different VHH-CARs, we tested Jurkat cells with stable expression of 5 different CD22-specific VHH CARs, a murine anti-CD19-scFv CAR (FMC63), or a human CD22-scFv CAR (m971). While the anti-CD3 mAb OKT3 was able to activate all CAR-expressing cells and WT Jurkat cells as expected, plate-bound anti-VHH mAb resulted in varying activation of all VHH CARs but not scFv or WT Jurkat cells (Fig. 7C). Generally, the 3H12 mAb resulted in a slightly more potent activation relative to 2A3, but a mixture of both mAbs resulted in activation of all Jurkat VHH-CAR cell lines, with slightly lower potency than plate-bound anti-CD3 OKT3 mAb.

To examine whether plate-bound anti-VHH mAb could similarly activate healthy donor CAR-T cells, we generated CAR-T cells expressing four different CD22-VHH CARs or a control CD22-scFv CAR via lentiviral transduction of T cells isolated from healthy donor leukapheresis samples. At day 12 after initial CD3/CD28 polyclonal activation and CAR-transduction, cells were initially cryopreserved for later analysis. In this case, a fluorescent marker (mNeonGreen) was co-expressed to identify CAR-expressing cells. VHH-CAR or control cells were thawed and stimulated with plate-bound 3H12 mAb, resulting in a visible phenotypic change by 24 hours in VHH-CAR expressing CAR-T cells stimulated with anti-VHH mAb but not for scFv-CAR-T or untransduced control T cells (Fig. 7D). Expression of the CD69 activation marker was increased in a dose-dependent manner for anti-VHH mAb stimulated VHH-CAR expressing cells but not scFv-CAR or control T cells (Fig. 7E). Over time, anti-VHH mAb stimulated VHH-CAR-T but not control cells showed a strong increase in GFP signal, formed large clumps of cells, and began proliferating (Fig. 8F, Supplemental Videos 1–6). At day 6 after anti-VHH mAb stimulation, cells were split to a low density in larger culture vessels with IL7 and IL15 cytokine supplementation. At day 22, anti-VHH mAb-expanded CAR-T products were assessed, revealing between 488 and 938-fold increase in total cell yield with >94% VHH-CAR expression. Anti-VHH mAb stimulation resulted in expansion of both CD8 and CD4 CAR-T cells, with a higher proportion of CD8 cells than the starting CAR-T product (Table 1). We also confirmed selective expansion of VHH-CAR expressing cells after anti-VHH stimulation, resulting in >90% CAR+ cells after anti-VHH expansion for all except one CAR molecule. Overall cell yield was much lower for PBMC CAR-T cells than for CAR-T leukapheresis.

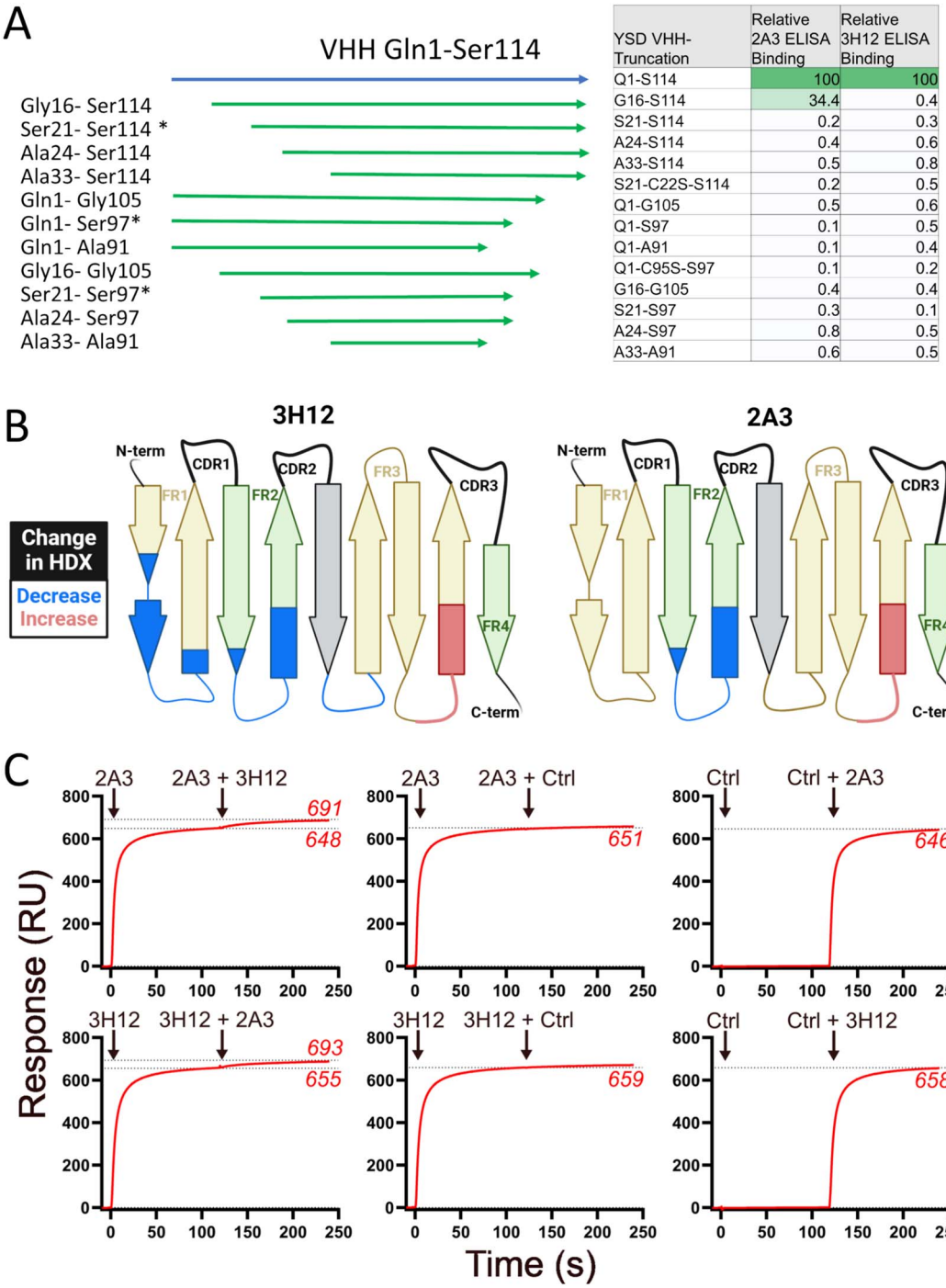

YSD VHH-Truncation	Relative 2A3 ELISA Binding	Relative 3H12 ELISA Binding
Q1-S114	100	100
G16-S114	34.4	0.4
S21-S114	0.2	0.3
A24-S114	0.4	0.6
A33-S114	0.5	0.8
S21-C22S-S114	0.2	0.5
Q1-G105	0.5	0.6
Q1-S97	0.1	0.5
Q1-A91	0.1	0.4
Q1-C95S-S97	0.1	0.2
G16-G105	0.4	0.4
S21-S97	0.3	0.1
A24-S97	0.8	0.5
A33-A91	0.6	0.5

Figure 4. Anti-VHH mAbs 3H12 and 2A3 bind to unique but adjacent epitopes. (A) YSD was used to map binding; inset table shows the % binding of anti-VHH mAbs via yeast whole-cell ELISA, normalized to the full-length VHH. (C) Hydrogen-deuterium exchange mass spectrometry was performed on purified VHH alone or bound to excess anti-VHH mAbs; VHH domain-wire diagram shows regions of significantly reduced (*blue*) or increased (*red*) hydrogen exchange when a VHH test material (1ug36) was saturated with 2A3 or 3H12 anti-VHH mAb. (C) Competitive SPR was performed using an amine coupled VHH, and mAbs were sequentially injected binding of the first anti-VHH mAb prevented most but not all binding of the second mAb, regardless of injection order, an irrelevant non-VHH binding mAb was included as a control ("ctrl"; cetuximab).

Overall, these data demonstrate that anti-VHH mAbs can be used to produce a selectively expanded VHH-CAR-T cell product.

Anti-VHH mAb expanded VHH-CAR-T cells maintain antigen-specific functionality and long-term response potential

We finally tested the functionality of CAR-T cells after anti-VHH mAb expansion using co-culture with varying target cells (Fig. 8A). First, to examine the short-term response of CAR-T cells with or without anti-VHH mAb activation, CAR-T cells were placed in co-culture with CD22+ Ramos cells at varying effector to target ratios for 7 days. We observed that anti-VHH mAb-expanded cells maintain similar or better killing of CD22+ target cells as non-activated CAR-T cells (Fig. 8B, Supplemental Fig. 5A). To test the persistence of cells expanded with anti-VHH mAbs, we examined growth in longer-term exhaustion-inducing conditions, wherein additional

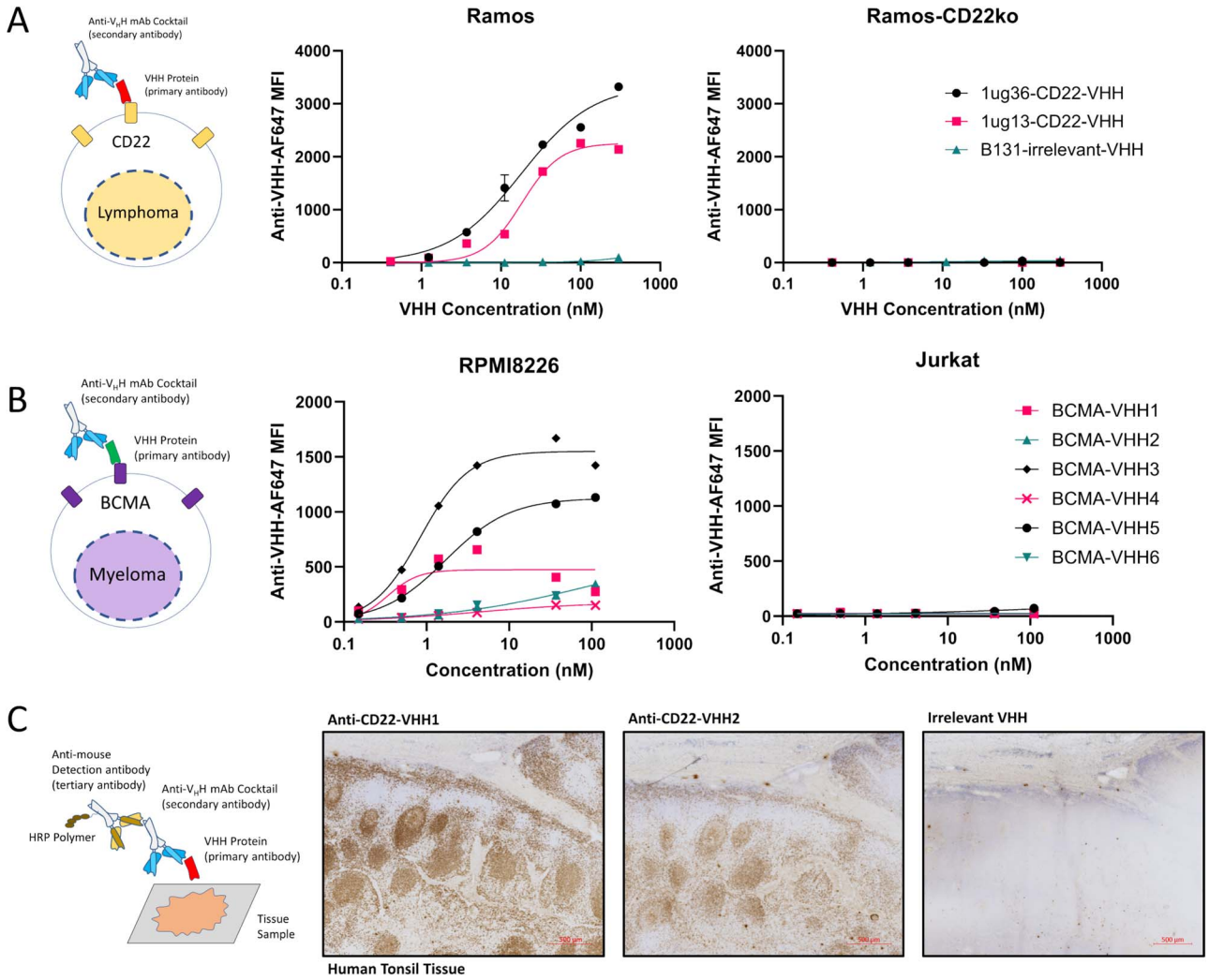

Figure 5. Anti-VHH mAbs can be used to assess cell and tissue binding of novel VHHs. (A) A human lymphoma cell line with high expression of CD22 (Ramos) or a similar line wherein CRISPR gene targeting was used to knockout CD22 expression (Ramos-CD22ko) was stained with purified CD22-specific VHHs (1ug36 or 1ug13 clones) or a control VHH of irrelevant specificity (B131), cells were then washed and stained with a mix of AlexaFluor-647 conjugated anti-VHH secondary mAb cocktail (3H12 and 2A3), and cells were examined via flow cytometry. (B) To demonstrate the general utility of this approach for VHHs of unknown sequence identity and cellular reactivity, a panel of BCMA-specific VHHs was similarly tested for reactivity to a BCMA+ multiple myeloma cell line (RPMI8226) or a BCMA-negative control cell line (Jurkat), followed by secondary staining with an anti-VHH cocktail. (C) To examine whether a similar approach can be used for assessment of tissue-level reactivity of VHHs, human tonsillar tissue known to have a high density of CD22+ B cells was stained with CD22-specific VHH, tissue was then stained with 3H12 anti-VHH mAb, and a tertiary anti-mouse HRP polymer detection reagent; images show expected follicular tissue distribution consistent with CD22-specific reaction.

target cells were added to co-cultures twice per week, and cultures were split weekly for 3 weeks. As expected, we observed that VHH-CAR-T cells display exhaustion under these conditions, with red-fluorescent target cells dominating the co-cultures at weeks 2 and 3 (Fig. 8C, Supplemental Fig. 5B). Interestingly, a benchmark m971 scFv-based CAR-T, which has been engineered for increased tonic signaling [17], shows only transient exhaustion, regaining capacity to restrict target cell growth at week 3 of co-culture. Examining the long-term response in anti-VHH mAb expanded VHH-CAR-T cells, we were surprised to also observe resistance to exhaustion, with CAR-T dominated co-cultures at week 3 with anti-VHH mAb-activated effector cells (Fig. 8C, Supplemental Fig. 5B). Importantly, anti-VHH mAb-expanded CAR-T cells do maintain antigenic selectivity, as no long-term restriction of CD22-knockout lymphoma or CD22-negative lung cancer cells was observed. In conclusion, we report that anti-VHH mAb expansion produces CAR-T cells that maintain strong short-term functionality and have potential for long-term antigen-specific responses.

Discussion

In this work, we report the development of a standardized Ab reagent for directly labeling and manipulating VHH CAR-T cells. In recent years, we have reported on our pre-clinical development of novel camelid VHH-based CARs targeting CD22 (10) and EGFR [11], and we are actively working on similar VHH-CAR therapeutics targeting BCMA, CD20, mesothelin, and other cancer-associated antigens. The broad reactivity of the anti-VHH mAb labeling reagents allows us to apply this tool across diverse VHH-CAR discovery projects, directly confirming surface expression during early VHH-CAR high-throughput screening [18], and obviating the need for a fluorescent marker in CAR-screening plasmids.

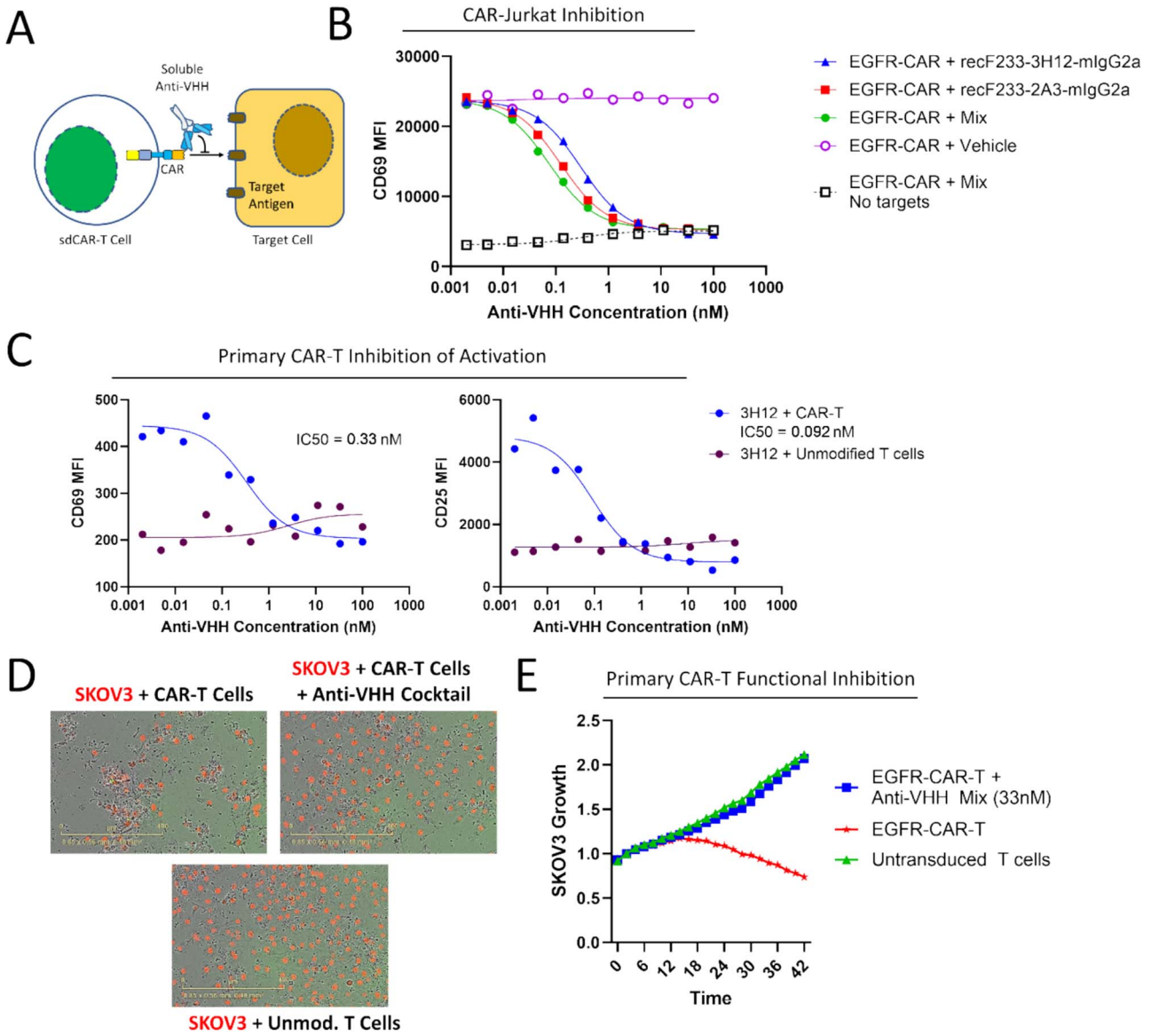

Figure 6. Soluble anti-VHH mAbs can block CAR-T cell responses. (A-B) To test the effect of soluble anti-VHH mAbs, EGFR-specific VHH-CAR expressing Jurkat cells were combined with EGFR-expressing target cells and varying doses of anti-VHH mAbs separately or as a cocktail, incubating co-cultures for 48 hours before assessing CAR-Jurkat cell activation via CD69-staining and flow cytometry. (C) A similar experiment was performed with lentivirally transduced primary human CAR-T cells, wherein upregulation of both CD69 and CD25 activation markers was diminished in a dose-dependent manner with a soluble anti-VHH mAb. (D) Primary CAR-T cells in co-culture with red-fluorescent protein-expressing EGFR-high SKOV3 target cells were examined for target cell survival via live fluorescence microscopy using an Incucyte device; images show a clear loss of target cells when co-cultured with EGFR-specific VHH CAR-T cells (top left) but not unmodified human T cells (bottom), or in the presence of soluble anti-VHH mAb treatment (right image). (E) Quantitation of red fluorescent signal over time, as measured via Incucyte, showing that anti-VHH mAb treatment completely blocks CAR-T specific lysis of target cells.

The anti-VHH mAbs we have developed are functionally analogous to anti-idiotypic mAbs against FMC63, the most common CD19-scFv used in CARs [19], aptamers specific for the FMC63 element of CD19-CARs [20], or fluorophore-tagged antigens. In contrast to such Ab or antigen-specific strategies, the anti-VHH mAbs reported here can be applied for detecting expression of VHH CAR targeting any antigen. Other, more generalized strategies for labeling CAR molecules, such as using fluorescent protein A, anti-linker Abs, and polyclonal anti-variable domain Abs [21], are less applicable to VHH-CARs; protein A reacts with only a subset of VHH molecules, and VHH-CARs lack the typical G4S or Whitlow linkers used in scFv-based CARs. While polyclonal anti-VHH Abs are now available, the lack of consistency and characterization of defined products can make pre-clinical and clinical development using such reagents challenging. The data presented here demonstrate that our dual-clonal anti-VHH mAb cocktail (3H12 and 2A3 mix) is a stable and consistent product, even after fluorophore conjugation, which could be applied in various high-quality release assays of pre-clinical and clinical-grade VHH-CAR cell and viral products.

In order to maximize the potential utility of our anti-VHH mAbs, we performed extensive characterization. Our epitope mapping results delineate two unique CDR-distal FR epitopes recognized by these mAbs, which impart advantages for the broader application of the mAb cocktail. Deuterium exchange results along with competitive SPR inhibition for mAb 3H12

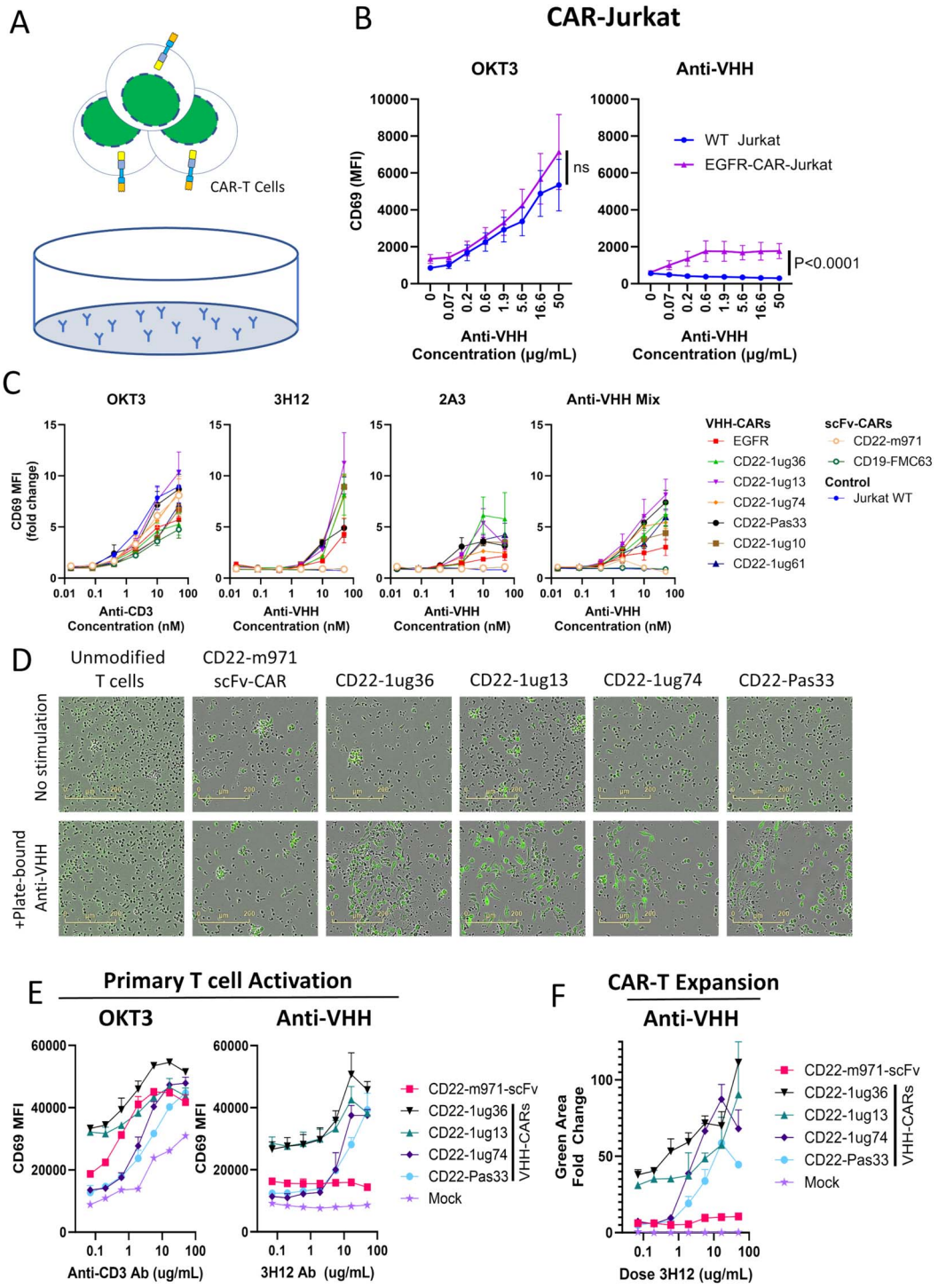

Figure 7. Immobilized anti-VHH mAbs can be used to activate and expand VHH-CAR-T cells. (A) Schematic of experimental setup to test whether plate-bound anti-VHH mAbs were able to activate VHH-CAR expressing cells. (B) Varying concentrations of anti-VHH mAbs were absorbed to a 96-well plate overnight, before washing and addition of CAR-Jurkat cells for an additional 24 hours; cells were then stained with CD69 antibody and assessed via flow cytometry. (C) To confirm this effect across varying cells expressing various VHH-CAR constructs, CAR-Jurkat cells were stimulated with plate-bound 3H12, 2A3, a mix of both anti-VHH mAbs, or plate-bound anti-CD3, and similarly examined for activation status via CD69 staining and flow cytometry. (D) A similar experimental setup was used to confirm that plate-bound anti-VHH mAbs can stimulate activation and proliferation of primary human CAR-T cells that co-express a green fluorescent marker (mNeonGreen). (E) Similarly, primary VHH CAR-T cells show upregulation of the CD69 activation marker and (F) expansion of green fluorescent marker co-expressed with the CAR transgene.

and 2A3 support distinct binding epitopes that are not entirely mutually exclusive and suggest close proximity to one another. The targeted epitopes here are contrary to a previously reported CDR-distal anti-VHH Fab domain [22] wherein binding involved a C-terminal tag. Amino acid sequence alignment of non-reactive and reactive VHHs revealed that there were several mutations unique to those VHHs not recognized by the mAb 3H12, including a serine residue at position 11 (as per the international

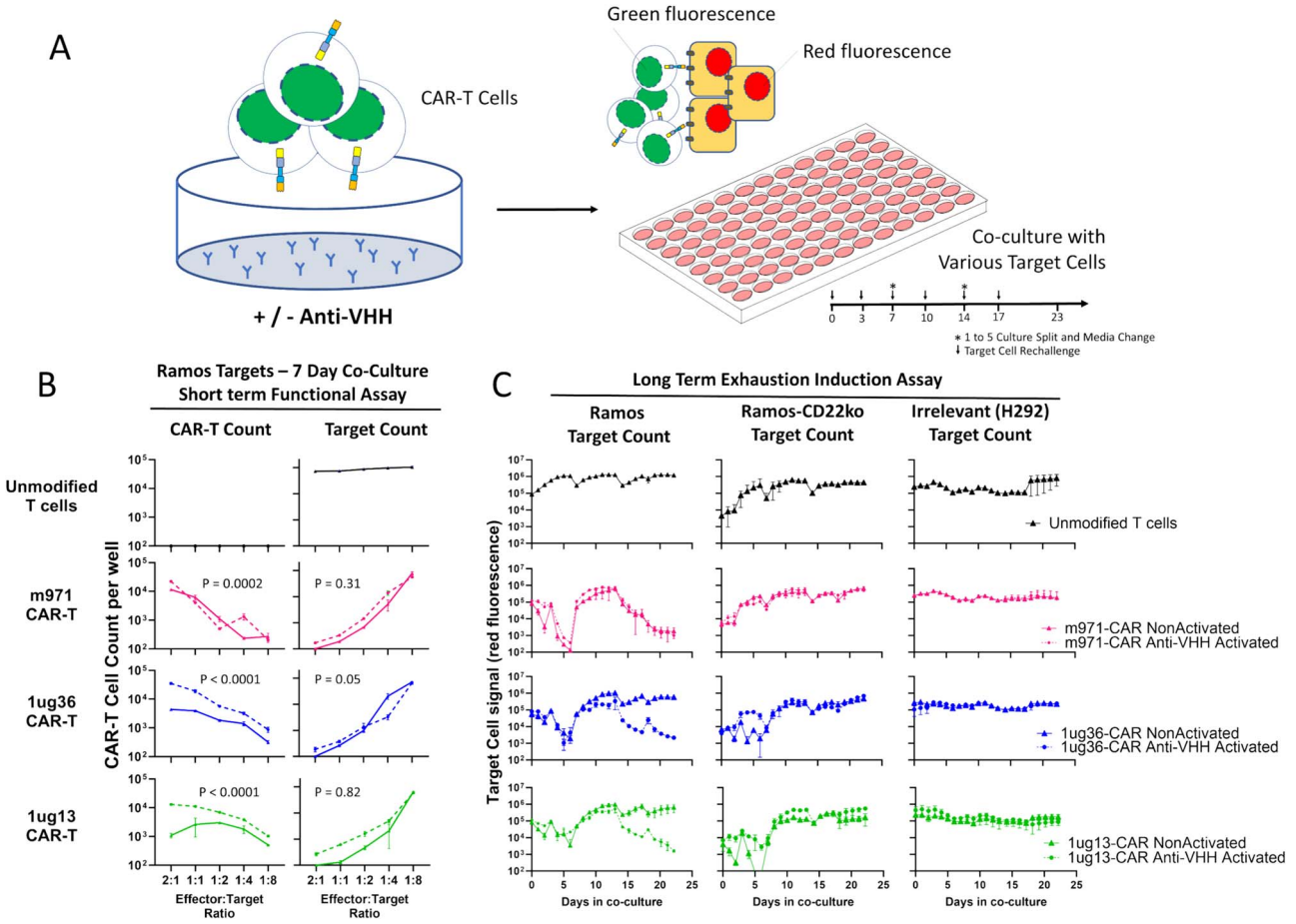

Figure 8. Functional testing of anti-VHH activated CAR-T cells. (A) Schematic of experimental setup to activate VHH CAR-T cells with plate-bound anti-VHH mAbs, followed by functional assay using co-culture with various target cells. (B) The short-term response to CD22+ Ramos target cells was examined across a range of effector to target ratios, wherein the number of red-fluorescent target cells and green-fluorescent CAR-T cells was enumerated using flow cytometry after 7 days of co-culture; inset *P* values show two-way ANOVA comparison of overlaid curves in graphs. (C) Co-cultures of 20 000 CAR-T cells with an equal number of CD22+ Ramos, CD22-knockout Ramos, or CD22-negative H292 lung cancer target cells; to drive CAR-T exhaustion, additional target cells were added to cultures at days 3, 7, 10, 14, and 17; 1 to 5 media exchanges and cell culture splits were also performed on days 7 and 14, = monitoring growth of red-fluorescent target cells via live regular fluorescent microscopy. All graphs show the response of non-activated CAR-T cells (solid lines) versus anti-VHH activated cells (broken lines) from a single experiment.

Table 1. Expansion of VHH CAR-T samples using plate-bound anti-VHH mAb.

		At CAR-T harvest			After anti-VHH mAb expansion				
[Donor]	**CAR**	**%CAR+ (GFP)**	**%CD8+**	**%CD4+**	**%CAR+ (GFP)**	**%CD8+**	**%CD4+**	**Total cells**	**Fold CAR+ growth**
Donor 1	Unmodified T cells	0.38	22.1	60.5	0.02	4.7	19.1	315 000	20
	CD22-m971 scFv	32	11.2	58.2	56.5	42.3	5.27	680 000	43
	CD22-1ug36	24.4	7.8	66.9	97.2	26.7	51.9	12 800 000	800
	CD22-1ug13	33.6	8.6	62.8	96	28.6	47.6	15 000 000	938
	CD22-1ug74	36	12.7	78.5	94.8	37.4	23.9	7 800 000	488
	CD22-Pas33	36	12.3	60.5	94.7	14.8	52.3	11 100 000	694
Donor 2	Unmodified T cells	0.04	14.3	33.6	5.1	66.8	8.8	*Not countable*	N/A
	BCMA-A6	53.5	11.6	62.2	86.1	20.3	47.3	825 000	7.7
	BCMA-H2	51.5	11.5	63.4	93.6	33.5	45.5	3 000 000	29
	BCMA-H4	68.9	14.2	60	90.5	43.5	39.4	1 000 000	7.3
Donor 3	Unmodified T cells	0.03	58.4	22.2	0	43.1	11.9	*Not countable*	N/A
	BCMA-A6	9.4	69.3	11.4	76.3	73.5	5.4	393 600	15
	BCMA-H2	14.5	66.6	20.4	90.1	74	12.5	2 406 200	75
	BCMA-H4	17.2	65.1	15.9	90.8	73.7	10.1	1 221 500	32

immunogenetics information; IMGT numbering system) in the VHH FR1 domain, wherein mutational reversion (S11L) fully restored 3H12 binding. While we were not able to pinpoint key interaction residues for the 2A3 mAb, our results clearly demonstrate that a dual-clonal anti-VHH mAb mix is applicable for VHH binding to the majority of VHHs, with the mixture of mAbs recognizing 75 out of 76 llama-derived VHHs tested. Anti-VHH mAb binding results confirm reactivity with llama and alpaca serum, two species known to have VHH Abs with highly similar FR regions [23]. Our data also confirm preferential binding to VHH over conventional VH/VL Abs, which are also found in llama and alpaca, with no reaction to human or mouse Abs. Based on this and epitope mapping results, we expect anti-VHH mAbs should be similarly reactive to species with VHH, which we have not yet tested (dromedary camel and bactrian camel).

In addition to surface labeling, we found that anti-VHH mAbs can block VHH-CAR reaction against antigen-positive target cells. A similar effect has been previously reported with anti-idiotypic Abs against CD19-CAR [19], and is analogous to the effect of anti-CD3 mAb blockade of T-cell receptor-mediated immune responses [24]. We believe this represents the first Ab product that has been demonstrated to be useful for direct blockade of VHH-CAR activation. Given that anti-VHH mAb epitopes are CDR-distal, and reactivity does not disrupt VHH-antigen interaction in cell labeling experiments, we infer that the mechanism of VHH-CAR disruption is likely through inhibition of CAR clustering or other downstream signaling mechanisms. These CAR-blocking mAbs could prove useful for investigating the nature of VHH-CAR signaling or to identify the optimal signaling magnitude and timing to increase CAR therapeutic efficacy *in vitro* or *in vivo*. Generating an infusible product derived from these anti-VHH mAbs could also have clinical utility, as it could conceivably allow for rapid and titratable blockade of VHH-CAR activity if and when toxicity is observed.

Another intriguing application of the anti-VHH mAbs reported here is the specific expansion of VHH-CAR-expressing T cells. Various techniques for expansion of CD19 CAR-T cells have been established previously, including stimulation with antigen-expressing artificial antigen-presenting cells [25, 26], antigen-bearing vesicles [27, 28], and multimerized target antigen [29]. While these strategies are proven to generate highly functional CAR-T products, they are target-antigen specific and thus cannot be broadly applied to novel CAR-T products. In contrast, stimulation with plate-bound anti-VHH mAbs is a target-agnostic approach capable of producing >500-fold CAR-T expansion, while maintaining CD4/CD8 heterogeneity and antigen-specific CAR-T functionality.

It is well documented that repeated stimulation through CD3 can lead to functional exhaustion of T cells (reviewed in [30]), and recent developments favor shortened manufacturing strategies with less CAR-T expansion to improve long-term persistence of CAR-T therapies [31, 32]. Given this, we were concerned whether anti-VHH mAb expansion could lead to functional exhaustion of VHH-CAR-T cells. In contrast to our initial hypothesis, our *in vitro* assessments indicate that anti-VHH mAb expanded cells maintain strong target-specific activity and appear to be resistant to exhaustion-inducing conditions. While these initial results are encouraging with regard to the use of anti-VHH mAbs to produce larger numbers of functional CAR-T cells, further experiments will be needed to characterize cellular signaling induced through stimulation with immobilized anti-VHH mAbs and the downstream transcriptional effect in CAR-T cells. In pursuit of this, we are currently developing a more refined and consistent method to expand VHH-CAR-T cells using bead-bound anti-VHH mAbs and investigating the potency of expanded CAR-T products in xenograft mouse models.

Overall, we have demonstrated that the new anti-VHH mAbs presented here are highly useful tools for labeling and manipulating VHH-CAR expressing cells, which could be of significant utility to the growing body of researchers working toward the development of more advanced VHH-CAR therapeutics.

Materials and methods

Mouse immunization

All of the animal work was monitored and approved by the National Research Council's Human Health Therapeutics Research Centre (NRC-HHT) Institutional Animal Care Committee and was conducted in accordance with the Canadian Council of Animal Care (CCAC) guidelines. Four six-week-old female A/J mice (The Jackson Laboratory, USA, Cat#000646) were bled (pre-immune serum) and injected intraperitoneally and subcutaneously with 100 μg of VHH antigen emulsified in TiterMax adjuvant (Cedarlane Labs, Canada, Cat#R-5) at day 0 and in phosphate-buffered saline (PBS) without adjuvant at day 26. Blood was collected in Microvette CB 300Z (Sarstedt, Canada, Cat#16-440) at day 33, and serum was stored at −20°C until further use. Pre- and post-immune sera titer of animals immunized with VHH antigen were assessed by ELISA. Unless otherwise stated, all incubations were performed at room temperature. Briefly, half-area 96-well plates (Costar, USA, Cat#3690) were coated with 25 μl per well of VHH at 5 μg/ml in PBS and incubated overnight at 4°C. Microplates were washed three times in PBS and blocked for 30 minutes with PBS containing 1% bovine serum albumin (BSA, Sigma, USA, Cat#A7030). Blocking buffer was removed and 25 μl of serial dilutions of sera samples were added. After a 2-hour incubation, microplates were washed four times with PBS-Tween 20 0.05% and 25 μl of a 1/5000 dilution of alkaline phosphatase conjugated goat anti-mouse IgG (H + L) (Jackson ImmunoResearch, Cat#115-056-062) in blocking buffer was added. After a 1-hour incubation, microplates were washed four times and 25 μl of p-nitrophenyl phosphate (pNPP) substrate (Sigma, USA, Cat#N7653) at 1 mg/ml in carbonate buffer at pH 9.6 was added and further incubated for 30 minutes. Absorbance was read at 405 nm using a SpectraMax plate reader (Molecular Devices, USA). All pre-immune bleeds were negative and all post-immune bleeds were very strong (above 1/12 800) on immunogen.

Hybridoma generation

After 2–3 months, an i.p. booster injection (100 μg of FC5-MOD protein produced in-house, in PBS) was done 3 days prior to fusion experiment. Spleen cells were harvested in Iscove's Modified Dulbecco's medium (IMDM, Gibco, USA, Cat#31980-030) and fused to NS0 myeloma cell line using polyethylene glycol. Spleen cells and myeloma cells were washed in IMDM, counted in RBC lysing buffer (Sigma, USA, Cat#7757-100ML), and mixed together at a 5:1 ratio. Pelleted cells were fused together by adding 1 ml of a 50% solution of PEG 4000 (EMD-Millipore Cat#9727-2) in PBS preheated at 37°C drop-wise over 1 minute, and incubated at 37°C for an additional 90 seconds. The reaction was stopped by addition of 30 ml of IMDM at 22°C over a period of 2 minutes. After a 10-minute incubation, freshly fused cells were spun at 233 g for 10 minutes. Cells were washed once in IMDM supplemented with 10% heat-inactivated fetal bovine serum (FBS) [Sigma Cat #F1051].

Following fusion, cells were suspended at a concentration of 2 × 10^5 input myeloma cells per ml in HAT selection medium (IMDM containing 20% heat inactivated FBS, penicillin–streptomycin (Sigma, USA, Cat#P7539), 1 ng/ml mouse IL-6 (Biolegend, USA, Cat#575706), HAT media supplement (Sigma, USA, Cat#H0262) and L-glutamine (Hy-Clone Cat#SH30034.01) and incubated at 37°C, 5% CO_2. The next day, hybridoma cells were washed and suspended at a concentration of 2–3 × 10^5 input myeloma cells per ml in semi-solid medium D (StemCell Technologies, Canada, Cat. No. 03804) supplemented with 5% heat inactivated FBS, 1 ng/ml mouse IL-6 and 10 μg/ml FITC- F(ab')2 Goat anti-mouse IgG (Jackson Immunoresearch, USA, # 115-096-071). The cell mixture was plated in an Omnitray dish (Nunc, USA, Cat#242811) and further incubated for 6–7 days at 37°C, 5% CO_2. Fluorescent secretor clones were then transferred using a mammalian cell clone picker (ClonepixFL, Molecular Devices, USA) into sterile 96-well plates (Costar, USA, #3595) containing 200 μl of IMDM supplemented with 20% heat inactivated FBS, penicillin–streptomycin, 1 ng/ml mouse IL-6, HT media supplement (Sigma, USA, Cat# H0137) and L-glutamine and incubated for 2–3 days at 37°C, 5% CO_2.

ELISA on hybridoma supernatants

Hybridoma supernatants were screened by ELISA to detect specific binders. To this end, 96-well half-area plates (Costar, USA #3690) were coated with 25 μl of FC5-MOD or FC5 derivatives FC5-VHH or FC5-hFc-1X0, or P257 (unrelated VHH) or EG2-hFc-X2 (unrelated VHH) or BSA (negative control) at 5 μg/ml in PBS and incubated overnight at 4°C. Microplates were washed three times with PBS, blocked with PBS-BSA 1%, and 25 μl of hybridoma supernatants were added and incubated at 37°C, 5% CO_2 for 2 hours. Plates were washed four times with PBS-Tween 20 0.05% and incubated for 1 hour at 37°C, 5% CO_2 with 25 μl of secondary antibody alkaline phosphatase conjugated F(ab')2 goat anti-mouse IgG Fc-gamma specific (Jackson Immunoresearch, USA, # 115-056-071) diluted 1/3000 in blocking buffer. After four washes with PBS-Tween 20 0.05%, 25 μl of a 1 mg/ml pNPP substrate solution was added and further incubated for 1 hour at 37°C. OD405nm measurements were done using a microplate reader (Spectramax® 340 PC, Molecular Devices, USA). Hybridoma supernatants were further analyzed for positive reactivity to various VHHs: VHH immunogen, 1ug13, and 1ug36; and for negative reactivity to human Abs using protX-hIgG (negative control).

Recombinant antibody production and purification

The VH and VL of each mAb were sequenced by Sanger sequencing, determining the CDRs sequence was determined using Kabat CDR numbering system. The VH and VL regions from 2A3 and 3H12 were cloned as fusions with mouse IgG2a/kappa constant regions (mouse IgG2a heavy chain and mouse kappa light chain, respectively) into the in-house pTT109 plasmid vector. Chinese hamster ovary (CHO) cells were then transfected with VL and VH containing constructs (1:1 ratio). Conditioned medium (CM) was harvested on day 7, recombinant Abs were purified on Protein A (HiTrap MabSelect SuRe, Cytiva, USA) connected to an AKTApure or an AKTAavant, buffer exchanged in DPBS on HiPrep™ desalting column (Cytiva, USA) connected to an AKTAexplorer, sterile-filtered, quantitated using a Nanodrop 2000 system, and evaluated by UPLC-SEC and SDS-PAGE. AF647 labeling was performed using a commercial kit (Invitrogen, USA, Cat#A20173), according to manufacturer's instructions.

VHH expression and purification

VHHs were expressed from pMRO.BAP.his plasmid in *Escherichia coli* BL21(nG3) using standard conditions. VHHs were isolated from the bacteria cell pellet by sonication in IMAC binding buffer, and lysates were cleared by centrifugation and filtration through a 0.2 mm PES filter. Each VHH was affinity-purified using His-TrapHP columns (Cytiva, USA) and gradient imidazole elution on an AKTAxpress (GE Healthcare, USA). His-purified VHHs were buffer exchanged to PBS using centrifugal filters (Amicon, USA) and further purified using a Superdex 75 Increase 10/300 GL size exclusion chromatography (SEC–Cytiva, USA) column connected to an AKTApurifier (GE Healthcare, USA).

ELISA detection of VHHs with anti-VHH mAbs

VHHs were diluted to 10 μg/ml in PBS and 1 μg VHH was absorbed to each uncoated ELISA well at 4°C overnight. All subsequent steps were performed at room temperature. Wells were blocked with 5% (w/v) skim milk in PBS for 1 hour; followed by incubation with 1:5000 anti-VHH mAb (3H12 and 2A3) in blocking buffer for 1 hour; 3× washing with PBS + 0.05% Tween 20; incubation with 1:5000 HRP conjugated donkey anti-mouse-IgG (Jackson Labs, Cat#715-035-150) in blocking buffer for 1 hour; 3× washing with PBS + 0.05% Tween20; and incubation with TMB substrate (Abcam, USA) for 5 minutes before stopping the reaction with 1 M phosphoric acid.

Surface plasmon resonance binding assays

All SPR experiments were conducted at 25°C on a Biacore T200 instrument (Cytiva, Canada) in PBST running buffer (135 mM NaCl, 2.7 mM KCl, 4.3 mM Na_2HPO_4, 1.4 mM KH_2PO_4, 3 mM EDTA, 0.05% (v/v) Tween 20, pH 7.2). For measurement of VHH monovalent affinities to 3H12 and 2A3 mAbs, ~2000 response units (RUs) of goat-anti-mouse IgG Fc (Jackson ImmunoResearch, USA, Cat#115-005-071) were amine coupled on a CM5 series S sensor chip (Cytiva) in 10 mM acetate buffer, pH 4.5, prior to capture of 3H12 or 2A3 mAbs (100 μg/ml) at 10 μl/minute flow rate and 60 seconds contact time. VHHs, previously purified by SEC, were injected at concentrations ranging from 2 to 1000 nM over captured 3H12 and 2A3 surfaces at a flow rate of 20 μl/minute, with 180 seconds of contact time and allowed to dissociate for 600 seconds. Surfaces were regenerated with 10 mM glycine, pH 1.5, at 30 μl/minute for 120 seconds. Reference flow cell subtracted single-cycle kinetics data was fit to a 1:1 interaction model using BIAevaluation 3.2 software (Cytiva, USA). For SPR competition experiments, a VHH (1ug36) that was recognized by both 3H12 and 2A3 mAbs was amine-coupled (135 RUs) on a CM5 series S sensor chip as above. Next, 3H12 (500 nM) was injected at 20 μl/minute for 120 seconds, followed immediately by injection of a mixture of 3H12 (500 nM) + 2A3 (500 nM) for 120 s. The reverse order (2A3 at 500 nM, followed by a mixture of 2A3 + 3H12, both at 500 nM) and injections with an irrelevant, non-VHH binding mAb (500 nM) were also performed. Surfaces were regenerated with 10 mM glycine, pH 1.5, at 100 μl/minute for 60 seconds, followed by 1 M $MgCl_2$ at 10 μl/minute for 10 seconds. For conditions where an irrelevant control antibody was tested, a research-grade source of EGFR-specific antibody, cetuximab (ThermoFisher Cat#LT600), was used.

VHH YSD and anti-VHH mAbs binding

Recombinant anti-VHH mAbs were examined for reactivity with truncated mutants of CD22-specific VHH 1ug36 generated as yeast-surface displayed fusion proteins (Aga2-HA-(VHH)-MYC).

Yeast cells were then grown under the inducing conditions in galactose media. The binding of the mAbs to yeast cells was performed using a whole yeast cell ELISA. Briefly, induced yeast cells were washed with 1 × PBS, and 1 × 10^6 cells were transferred per well to 96-well filter plate (#MSDVN6550 MultiScreen DV Filter Plate, Millipore). After adhering yeast cells, PBS was removed by vacuum aspiration, and 200 μl of blocking solution (PBS with 2% BSA and 0.05% Tween 20, Sigma Aldrich, USA) was added, and plates were incubated for 45 minutes at room temperature with shaking. Blocking solution was removed by vacuum aspiration and 100 μl of biotinylated anti-VHH mAbs (100–250 nM), or irrelevant mouse monoclonal anti-c-myc antibody (9E10) at 3 μg/ml (Sigma) was added and incubated for 1 hour at room temperature with shaking. Cells were washed 4× with 200 μl per well PBS + 0.05% Tween 20. Detection of biotinylated VHHs was performed using 100 μl of HRP-conjugated streptavidin (Jackson # 016-030-084) at 1/10000 dilution in 1% BSA + 1× PBS + 0.025% Tween 20, and MYC-tag was detected with 100 μl per well of HRP-F(ab)2 fragment goat anti-mouse IgG (H + L) (Jackson ImmunoResearch, Cat #115-036-062) at 1/5000 in the same binding solution. Mixture was incubated for 1 hour at room temperature with shaking, then washed 4 × with PBS + 0.05% Tween 20, followed by adding 100 μl per well of TMB substrate solution (Thermo Fisher, USA, Cat#34021) and incubated for 10 minutes at room temperature, before stopping with 0.2 M sulfuric acid. Absorbance at 450 nm (OD450) was measured using a Tecan Infinite M1000 Pro plate reader.

Serum fractionation

Whole normal serum was sourced from Cedarlane (llama, NRC project), Jackson ImmunoResearch (alpaca, 028-000-121), and the NRC Canada animal facility (mouse), and healthy human donors (collected under research ethics approved protocol at the Ottawa Hospital Research Institute). Serum was fractionated following standard methods [33]. Briefly, serum was flowed in tandem through a HiTrap Protein G column (GE Healthcare 71-7001-00 AP) followed by a HiTrap Protein A column (GE Healthcare 71-7002-00 AP) and serum Abs were eluted step-wise with citrate buffer, pH 3.5 and then glycine buffer, pH 2.7 (Protein G column to produce fractions G1 and G2, respectively) or sodium acetate buffer, pH 4.5 and then glycine buffer, pH 2.7 (Protein A column to produce fractions A1 and A2, respectively). Fractions were collected using an FPLC AKTA purification system (GE Healthcare), neutralized with Tris–HCl buffer, pH 8.8, and then dialyzed to phosphate buffer, pH 7.

Serum ELISA

Whole and fractionated serum were absorbed to uncoated ELISA wells in a three-fold titration from 4 μg/ml to 2 ng/ml. 1% casein was used for blocking, and all washes were performed three times with 0.05% Tween 20 in PBS. Coated and blocked ELISA wells were incubated with a biotinylated cocktail of anti-VHH Abs, 2A3 and 3H12 (1:3000), for 1 hour, then washed, incubated with HRP-conjugated streptavidin (1:5000, Jackson ImmunoResearch 016-030-084) for 1 hour, then washed, and developed with TMB ELISA substrate (Abcam ab171523) for 5 minutes before stopping the reaction with 1 M phosphoric acid.

Serum SDS-PAGE

Fractionated serum was analyzed by SDS-PAGE by loading 2 μg serum protein onto 4%–20% Mini-PROTEAN TGX Stain-Free Protein Gel (Bio-Rad 4,568,096) with Precision Plus Protein Unstained Protein Standard (Bio-Rad 1,610,363). Gel was visualized using a Gel Doc EZ Imager system (Bio-Rad).

HDX mapping

For HDX-MS, purified sdAb-1ug36 protein was equilibrated with a saturating concentration of each anti-VHH mAb (1:1 molar ratio). Deuterium labeling of the mAb-VHH complexes or VHH (1ug36 clone) alone was initiated by a two-fold dilution with deuterated buffer (PBS in 90% D_2O). A controlled time period of either 0.5 or 3 minutes was allowed before the reaction was quenched by a five-fold dilution with 1 M guanidine HCl, 40 mM TCEP in 0.1% formic acid at 4°C. Samples were then trapped (ACQUITY UPLC BEH C18 VanGuard Pre-column, 130 Å, 1.7 μm, 2.1 mm × 5 mm), washed, and digested with immobilized Nepenthesin-II (Affipro) at 100 μl/minute for 5 minutes (2°C). Peptides were eluted from an Acquity UPLC column (PST BEH C18, 130A, 1.7 μm, 100 μm × 100 mm) with a 1%–35% acetonitrile gradient (0.23% formic acid) at 40 μL/minute. Data was collected on a Synapt G2-Si mass spectrometer with ion mobility enabled (Waters). A peptide map was generated with a database search (Mascot) of a data-dependent acquisition of an unlabeled 1ug36 VHH sample. Deuteration was assigned in triplicate for 41 peptides covering 81% of the sdAb-1ug36 sequence using HDExaminer and Mass Spec [34] (Supplemental Fig. 2, Supplemental Table 2). Differential HDX was assessed by subtracting the deuterium content of the unbound (1ug36) from the mAb-VHH complex (2A3 or 3H12 + 1ug36). Significance was assessed using a two-state Welch's T-test with a 1-p threshold of 0.98 and a 3x standard deviation cut-off. Differences ($\Delta D = D_{mAb+VHH} - D_{VHH}$) in absolute (Δ #D) and relative (Δ % D) deuterium content are shown for each 1ug36 peptide. Relative data is normalized to the theoretical maximum deuterium of each peptide.

Cell binding and IHC

Highly pure CD22- or BCMA-specific VHHs, and a control VHH specific for an irrelevant bacterial toxin (B131; as reported in [35]), were produced using a standard bacterial expression system and metal affinity column purification. Myeloma (RPMI8226) or lymphoma (Ramos), or a modified cell line wherein CRISPR technology has been employed to specifically disrupt CD22 expression, were combined with varying concentrations of these purified VHH proteins. Cells were then washed and stained with the mixed AF-647-labeled 2A3 and 3H12 mAbs as a secondary antibody. Binding was then assessed via flow cytometry using an LSRFortessa flow cytometer (BD Bioscience, USA). IHC was performed using human tonsillar tissue, which was fixed using methanol/Acetone. Tissue sections were then stained with primary CD22 VHH1 or VHH2, washed, and probed with a secondary anti-VHH mAb. This was then washed again and stained with a tertiary anti-mouse-HRP polymer reagent as per manufacturer recommendation (Leica Biosystems, Canada, Cat#DS9800).

CAR-Jurkat activation or inhibition assays

For anti-VHH mAb inhibition assay, EGFR-CAR Jurkat cells were generated using lentiviral transduction as previously reported [11]. EGFR CAR-Jurkat were then placed at 37°C for 48 hours in co-culture with EGFR-positive SKOV3 human lung cancer cells, in the presence of decreasing concentrations of the anti-VHH mAbs 2A3 and 3H12, alone or in combination, or vehicle control. For activation studies, varying doses of anti-VHH mAbs were absorbed onto 96-well flat-bottom cell culture plates (Corning, USA, Cat#3595) overnight in PBS. Jurkat cells with stable expression of various CD22 VHH-CAR or scFv-CARs, as previously reported

[10] were then placed on the wells and incubated at 37°C and 5% CO_2 overnight. Cells were stained with anti-CD69-APC (BD Bioscience, USA, Cat#555533), washed, and examined via flow cytometry.

CAR-T generation, anti-VHH mAb inhibition or expansion, and functional testing

EGFR or CD22 primary CAR-T cells were generated from healthy PBMC or donor apheresis product, respectively, as previously described [11, 15]. For flow cytometric assessment of anti-VHH mAb candidates, cells were combined with a consistent amount of anti-VHH mAb supernatant, followed by washing and staining with AF647-labeled Goat-anti mouse Fab detection reagent (Jackson Immunoresearch Cat#115-607-003). For inhibition studies, EGFR CAR-T cells were placed at an E:T ratio of 1:1 with red fluorescent protein expressing (Nuclight Lenti-Red, Sartorius, USA) SKOV3 cells in the presence of absence of various doses of anti-VHH mAbs. The relative growth of CAR-T and target cells was then monitored over 42 hours using an Incucyte device (Sartorius, USA). For anti-VHH mAb expansion studies, 20 000 CD22 CAR-T cells were placed in a 96-well flat bottom plate which was coated with varying doses of anti-VHH mAbs. Cells were observed regularly using live fluorescence microscopy via Incucyte and flow cytometry at day 7. After 6 days in culture, anti-VHH mAb activated CAR-T cells were also transferred to larger growth vessels to allow for full proliferation.

For the functional experiments testing with or without plate-bound anti-VHH mAb stimulation, cryopreserved CD22 CAR-T cells generated from healthy donor apheresis product as previously reported were used [15]. CD22 CAR-T cells or matched untransduced control T cells were thawed and allowed to recover for 24 hours before stimulating with plate-bound anti-VHH mAbs in a 24-well plate as described in the text. Cells were incubated in Immunocult × F media supplemented with IL-7 and IL-15, in 24-well tissue culture plates coated overnight with or without anti-VHH mAbs. Cells were allowed to expand for 12 days, with removal of excess cells to tissue culture flasks with no anti-VHH mAb as cells reached confluency, maintaining between 2.5 to 5×10^5 cells per ml throughout the expansion period. For functional testing, cells were plated with target cells stably expressing Nuclight-Lenti-Red (Sartorius USA), with varying target cell types, and at varying effector to target ratios in Immunocult XF media supplemented with 100 U/ml IL-2, as described in the text. The relative growth of target and effector cells was examined using live fluorescence microscopy (Incucyte S3 device, Sartorius, USA). Every 2–3 days, additional target cells were added at equivalent numbers to initial challenge. Every 7 days, cultures were split 1–5 with fresh media, simultaneously with additional target cells. At weekly splits, flow cytometric analysis was used to enumerate and characterize co-cultures.

Author contributions

Scott McComb (Conceptualization [lead], Data curation [lead], Formal analysis [lead], Funding acquisition [lead], Methodology [lead], Project administration [lead], Resources [lead], Supervision [lead], Visualization [lead], Writing—original draft [lead], Writing—review & editing [lead]), Bianca Dupont (Formal analysis [supporting], Investigation [supporting], Writing—review & editing [supporting]), Alex Shepherd (Formal analysis [supporting], Investigation [supporting]), Bigitha Bennychen (Formal analysis [supporting], Investigation [supporting]), Anne Marcil (Conceptualization [equal], Formal analysis [equal], Investigation [equal], Methodology [equal], Writing—review & editing [equal]), Mehdi Arbabi-Ghahroudi (Conceptualization [equal], Data curation [equal], Formal analysis [equal], Investigation [equal], Methodology [equal], Project administration [equal], Supervision [equal], Writing—original draft [equal], Writing—review & editing [equal]), Laura Tamblyn (Investigation [supporting], Methodology [supporting]), Shalini Raphael (Investigation [supporting], Methodology [supporting]), Joey Sheff (Conceptualization [supporting], Formal analysis [supporting], Investigation [supporting], Methodology [supporting], Visualization [supporting], Writing—original draft [supporting], Writing—review & editing [supporting]), Greg Hussack (Formal analysis [supporting], Investigation [supporting], Methodology [supporting], Supervision [supporting], Visualization [supporting], Writing—review & editing [supporting]), Anna N. Moraitis (Formal analysis [supporting], Supervision [supporting], Visualization [supporting], Writing—review & editing [supporting]), Cunle Wu (Formal analysis [supporting], Investigation [supporting], Methodology [supporting], Supervision [supporting], Writing—review & editing [supporting]), Annie Aubry (Investigation [supporting], Methodology [supporting]), Christine Gadoury (Investigation [supporting], Methodology [supporting]), Julie Lippens (Investigation [supporting]), Martine Pagé (Investigation [supporting]), Annie Fortin (Investigation [supporting]), Simon Joubert (Investigation [supporting], Methodology [supporting], Supervision [supporting], Writing—review & editing [supporting]), Linda Lamoureux (Investigation [supporting]), Marie Parat (Investigation [supporting], Methodology [supporting], Supervision [supporting]), Pierre Plante (Investigation [supporting]), Félix Malenfant (Investigation [supporting]), Mauro Acchione (Investigation [supporting], Methodology [supporting], Supervision [supporting], Validation [supporting]), Petra Pohankova (Data curation [supporting], Formal analysis [supporting], Investigation [supporting], Writing—review & editing [supporting]), Joe Schrag (Formal analysis [supporting], Investigation [supporting], Methodology [supporting]), Andrea Acel (Investigation [supporting]), Mathieu Coutu (Investigation [supporting], Methodology [supporting]), Emma Smith (Investigation [supporting]), Majida El Bakkouri (Investigation [supporting], Methodology [supporting]), Jennifer J. Hill (Conceptualization [supporting], Formal analysis [supporting], Investigation [supporting], Methodology [supporting], Writing—review & editing [supporting]), Tammy-Lynn Tremblay (Investigation [supporting], Methodology [supporting]), Manceur Aziza (Formal analysis [supporting], Investigation [supporting], Methodology [supporting], Supervision [supporting]), Sharlene Faulkes (Investigation [supporting], Methodology [supporting], Writing—review & editing [supporting]), John Webb (Conceptualization [supporting], Formal analysis [supporting], Investigation [supporting], Methodology [supporting], Writing—review & editing [supporting]), Ahmed Zafer (Investigation [supporting], Methodology [supporting]), Qin Zhu (Investigation [supporting], Methodology [supporting]), Tina Nguyen (Conceptualization [supporting], Formal analysis [supporting], Investigation [supporting], Methodology [supporting], Project administration [supporting], Writing—review & editing [supporting]), Robert A. Pon (Conceptualization [supporting], Formal analysis [supporting], Funding acquisition [supporting], Investigation [supporting], Methodology [supporting], Writing—review & editing [supporting]), and Risini D. Weeratna (Conceptualization [supporting], Formal analysis [supporting], Funding acquisition [supporting], Investigation [supporting], Methodology [supporting], Project administration [supporting], Supervision [supporting], Writing—original draft [supporting], Writing—review & editing [supporting])

Supplementary data

Supplementary data is available at *ABT* online.

Conflict of interest

The anti-VHH antibodies reported here are the subject of a provisional patent application by the National Research Council of Canada.

Funding

This work was funded by the National Research Council Canada Disruptive Technology Solutions Cell and Gene Therapy challenge program and BioCanRx.

Data availability

All data related to this work is fully reported here. Requests for access to raw data or sequence information can be sent to the corresponding author and will be provided under reasonable agreement.

Ethics and consent statement

Human samples used here were collected at the Ottawa Hospital Research Institute, with donor consent and in accordance with research ethics board (REB)-approved oversight and an approved protocol.

Animal research statement

All of the animal work was monitored and approved by the National Research Council's Human Health Therapeutics Research Centre (NRC-HHT) Institutional Animal Care Committee and was conducted in accordance with the Canadian Council of Animal Care (CCAC) guidelines.

References

1. Van Wauwe JP, De Mey JR, Goossens JG. OKT3: a monoclonal anti-human T lymphocyte antibody with potent mitogenic properties. *J Immunol* 1980;**124**:2708–13. https://doi.org/10.4049/jimmunol.124.6.2708.
2. Chang TW, Gingras SP. OKT3 monoclonal antibody inhibits cytotoxic T lymphocyte mediated cell lysis. *Int J Immunopharmacol* 1981;**3**:183–6. https://doi.org/10.1016/0192-0561(81)90011-4.
3. Rinnooy Kan EA, Wright SD, Welte K. *et al.* Fc receptors on monocytes cause OKT3-treated lymphocytes to internalize T3 and to secrete IL-2. *Cell Immunol* 1986;**98**:181–7. https://doi.org/10.1016/0008-8749(86)90278-9.
4. van Lier RA, Brouwer M, Rebel VI. *et al.* Immobilized anti-CD3 monoclonal antibodies induce accessory cell-independent lymphokine production, proliferation and helper activity in human T lymphocytes. *Immunology* 1989;**68**:45–50.
5. Poltorak MP, Graef P, Tschulik C. *et al.* Expamers: a new technology to control T cell activation. *Sci Rep* 2020;**10**:17832.
6. Zhong K, Liu Z, Li H. *et al.* T cell stimulation and expansion by SunTag-based clustering of anti-CD3/CD28 scFv. *Aging* 2020;**12**:11061–70. https://doi.org/10.18632/aging.103318.
7. Zappasodi R, Nicola MD, Carlo-Stella C. *et al.* The effect of artificial antigen-presenting cells with preclustered anti-CD28/-CD3/-LFA-1 monoclonal antibodies on the induction of ex vivo expansion of functional human antitumor T cells. *Haematologica* 2008;**93**:1523–34. https://doi.org/10.3324/haematol.12521.
8. Levine BL, Bernstein WB, Connors M. *et al.* Effects of CD28 costimulation on long-term proliferation of CD4+ T cells in the absence of exogenous feeder cells. *J Immunol* 1997;**159**:5921–30. https://doi.org/10.4049/jimmunol.159.12.5921.
9. Muyldermans S. Applications of nanobodies. *Annu Rev Anim Biosci* 2021;**9**:401–21. https://doi.org/10.1146/annurev-animal-021419-083831.
10. McComb S, Weeratna R, Arbabi-Ghahroudi M. *et al. Anti-cd22 Single Domain Antibodies and Therapeutic Constructs* 2023.
11. McComb S, Nguyen T, Shepherd A. *et al.* Programmable attenuation of antigenic sensitivity for a nanobody-based EGFR chimeric antigen receptor through hinge domain truncation. *Front Immunol* 2022;**13**. https://doi.org/10.3389/fimmu.2022.864868.
12. Berdeja JG, Madduri D, Usmani SZ. *et al.* Ciltacabtagene autoleucel, a B-cell maturation antigen-directed chimeric antigen receptor T-cell therapy in patients with relapsed or refractory multiple myeloma (CARTITUDE-1): a phase 1b/2 open-label study. *The Lancet* 2021;**398**:314–24. https://doi.org/10.1016/S0140-6736(21)00933-8.
13. Abulrob A, Sprong H, En Henegouwen PVB. *et al.* The blood–brain barrier transmigrating single domain antibody: mechanisms of transport and antigenic epitopes in human brain endothelial cells. *J Neurochem* 2005;**95**:1201–14. https://doi.org/10.1111/j.1471-4159.2005.03463.x.
14. Sun Y, Gadoury C, Hirakawa MP. *et al.* Deletion of a Yci1 domain protein of Candida albicans allows homothallic mating in MTL heterozygous cells. *mBio* 2016;**7**:e00465–16. https://doi.org/10.1128/mBio.00465-16.
15. McComb S, Arbabi-Ghahroudi M, Hay KA. *et al.* Discovery and preclinical development of a therapeutically active nanobody-based chimeric antigen receptor targeting human CD22. *Mol Ther: Oncology* 2024;**32**:200775. https://doi.org/10.1016/j.omton.2024.200775.
16. Bertheloot D, Wanderley CW, Schneider AH. *et al.* Nanobodies dismantle post-pyroptotic ASC specks and counteract inflammation in vivo. *EMBO Mol Med* 2022;**14**:e15415.
17. Singh N, Frey NV, Engels B. *et al.* Antigen-independent activation enhances the efficacy of 41BB co-stimulated CD22 CAR T cells. *Nat Med* 2021;**27**:842–50. https://doi.org/10.1038/s41591-021-01326-5.
18. Bloemberg D, Nguyen T, MacLean S. *et al.* A high-throughput method for characterizing novel chimeric antigen receptors in Jurkat cells. *Mol Ther - Methods & Clinical Development* 2020;**16**:238–54. https://doi.org/10.1016/j.omtm.2020.01.012.
19. Jena B, Maiti S, Huls H. *et al.* Chimeric antigen receptor (CAR)-specific monoclonal antibody to detect CD19-specific T cells in clinical trials. *PloS One* 2013;**8**:e57838. https://doi.org/10.1371/journal.pone.0057838.
20. Zhou H, Abudureheman T, Zheng W-W. *et al.* CAR-aptamers enable traceless enrichment and monitoring of CAR-positive cells and overcome tumor immune escape. *Adv Sci* 2024;**11**:2305566.
21. Hu Y, Huang J. The chimeric antigen receptor detection toolkit. *Front Immunol* 2020;**11**. https://doi.org/10.3389/fimmu.2020.01770.
22. Wu X, Rapoport TA. Cryo-EM structure determination of small proteins by nanobody-binding scaffolds (Legobodies). *Proc Natl Acad Sci* 2021;**118**:e2115001118.

23. Vu KB, Ghahroudi MA, Wyns L. *et al.* Comparison of llama VH sequences from conventional and heavy chain antibodies. *Mol Immunol* 1997;**34**:1121–31. https://doi.org/10.1016/S0161-5890(97)00146-6.
24. Menon AP, Moreno B, Meraviglia-Crivelli D. *et al.* Modulating T cell responses by targeting CD3. *Cancers (Basel)* 2023;**15**:1189.
25. Butler MO, Hirano N. Human cell-based artificial antigen-presenting cells for cancer immunotherapy. *Immunol Rev* 2014;**257**:191–209. https://doi.org/10.1111/imr.12129.
26. Singh H, Figliola MJ, Dawson MJ. *et al.* Manufacture of clinical-grade CD19-specific T cells stably expressing chimeric antigen receptor using sleeping beauty system and artificial antigen presenting cells. *PloS One* 2013;**8**:e64138. https://doi.org/10.1371/journal.pone.0064138.
27. Ukrainskaya V, Rubtsov Y, Pershin D. *et al.* Antigen-specific stimulation and expansion of CAR-T cells using membrane vesicles as target cell surrogates. *Small* 2021;**17**:2102643.
28. Zhang Y, Ge T, Huang M. *et al.* Extracellular vesicles expressing CD19 antigen improve expansion and efficacy of CD19-targeted CAR-T cells. *IJN* 2023;**18**:49–63.
29. Hu Y, Cao G, Chen X. *et al.* Antigen multimers: specific, sensitive, precise, and multifunctional high-avidity CAR-staining reagents. *Matter* 2021;**4**:3917–40. https://doi.org/10.1016/j.matt.2021.09.027.
30. Jenkins E, Whitehead T, Fellermeyer M. *et al.* The current state and future of T-cell exhaustion research. *Oxf Open Immunol* 2023;**4**:iqad006.
31. Ghassemi S, Durgin JS, Nunez-Cruz S. *et al.* Rapid manufacturing of non-activated potent CAR T cells. *Nat Biomed Eng* 2022;**6**:118–28. https://doi.org/10.1038/s41551-021-00842-6.
32. Yang J, He J, Zhang X. *et al.* Next-day manufacture of a novel anti-CD19 CAR-T therapy for B-cell acute lymphoblastic leukemia: first-in-human clinical study. *Blood Cancer J* 2022;**12**:1–9.
33. Baral TN, MacKenzie R, Arbabi Ghahroudi M. Single-domain antibodies and their utility. *Curr Protoc Immunol* 2013;**103**:2.17.1–2.17.57. https://doi.org/10.1002/0471142735.im0217s103.
34. Rey M, Sarpe V, Burns KM. *et al.* Mass spec studio for integrative structural biology. *Structure* 2014;**22**:1538–48. https://doi.org/10.1016/j.str.2014.08.013.
35. Hussack G, Arbabi-Ghahroudi M, van Faassen H. *et al.* Neutralization of clostridium difficile toxin a with single-domain antibodies targeting the cell receptor binding domain. *J Biol Chem* 2011;**286**:8961–76. https://doi.org/10.1074/jbc.M110.198754.

Antibody Therapeutics, 2025, 8(3), 242–258
https://doi.org/10.1093/abt/tbaf011
Research Article